



Durham E-Theses

What Thy Right Hand Doeth: Simulating the Effects of Physics beyond the Standard Model on Earth-Traversing Ultra-High-Energy Neutrinos

HEIGHTON, ROBERT,ANTHONY

How to cite:

HEIGHTON, ROBERT,ANTHONY (2025) *What Thy Right Hand Doeth: Simulating the Effects of Physics beyond the Standard Model on Earth-Traversing Ultra-High-Energy Neutrinos*, Durham theses, Durham University. Available at Durham E-Theses Online: <http://etheses.dur.ac.uk/16004/>

Use policy

The full-text may be used and/or reproduced, and given to third parties in any format or medium, without prior permission or charge, for personal research or study, educational, or not-for-profit purposes provided that:

- a full bibliographic reference is made to the original source
- a [link](#) is made to the metadata record in Durham E-Theses
- the full-text is not changed in any way

The full-text must not be sold in any format or medium without the formal permission of the copyright holders.

Please consult the [full Durham E-Theses policy](#) for further details.

What Thy Right Hand Doeth

*Simulating the Effects of Physics beyond the
Standard Model on Earth-Traversing
Ultra-High-Energy Neutrinos*

Robert Heighton

A Thesis presented for the degree of
Doctor of Philosophy



Institute for Particle Physics Phenomenology
Department of Physics
Durham University
United Kingdom

March 2025

What Thy Right Hand Doeth

*Simulating the Effects of Physics beyond the
Standard Model on Earth-Traversing
Ultra-High-Energy Neutrinos*

Robert Heighton

Submitted for the degree of Doctor of Philosophy

March 2025

Abstract: Neutrinos of ultra-high energy (UHE)—that is, with energy of EeV (10^{18} eV) order and above—originate from cosmogenic processes and transient astrophysical events, and arrive at the Earth in fluxes that will be increasingly constrained and measured by next-generation large-volume observatories such as GRAND, POEMMA, PUEO, TAMBO, TAROGE-M, and Trinity. At such energies, the Earth is effectively opaque; a UHE neutrino shallowly skimming the Earth may exit, sometimes in the form of a τ whose decay in the atmosphere can be detected, while at deeper angles corresponding to longer distances through the Earth’s interior, a UHE neutrino cannot survive the journey with comparable energy.

In this thesis, I explore the influence that physics beyond the Standard Model (BSM) may have on the exit probabilities of UHE neutrinos traversing the Earth, and the signatures that such influence may produce in the observations and measurements of detectors. In particular, I introduce to this scenario a right-handed neutrino (RHN) in the form of a Majorana fermion of GeV-scale mass that mixes with the left-handed τ neutrino according to a mixing parameter θ_{mix} , and use Monte Carlo simulations adapted to include the relevant BSM interactions and decays to test this model’s

effects. I then simulate GRAND and POEMMA, two relevant future detectors, to predict the impact on their results.

It is found that, in light of a transient astrophysical event similar to GRB 221009 occurring within a vicinity of $\lesssim 1$ Mpc, a POEMMA-like detector in particular should be capable of probing this regime and providing complementary constraints on the BSM model, thus demonstrating that the observation of Earth-traversing UHE neutrinos at large-volume detectors has potential as an avenue for exploring and testing new physics.

Contents

Abstract	3
List of Figures	9
List of Tables	13
1 Introduction	23
1.1 Neutrinos and Ultra-High Energies	24
1.2 Probing Physics beyond the Standard Model	25
1.3 The Structure of this Thesis	26
2 The Standard Model and Beyond	29
2.1 The Standard Model of Particle Physics	29
2.1.1 The SM Gauge Group and Spontaneous Symmetry Breaking	30
2.1.2 The Higgs Mechanism and the Emergence of the Electroweak Gauge Bosons	31
2.1.3 Yukawa Interactions and Fermion Mass	33
2.1.4 A Good Theory	36
2.2 Neutrinos	37
2.2.1 A Brief History	37

2.2.2	Neutrinos in the Standard Model	40
2.2.3	Oscillation and Mass	41
2.3	Beyond the Standard Model	44
2.3.1	Missing Pieces	44
2.3.2	The Right-Handed Neutrino and Majorana Mass	45
2.4	The Model	47
2.4.1	Scatterings	48
2.4.2	Decays	49
3	UHE Neutrinos: A Journey through the Earth	53
3.1	Sources	53
3.1.1	Cosmogenic Neutrinos	54
3.1.2	Transient Astrophysical Sources	56
3.2	In the Earth	56
3.2.1	Neutrino-Nucleon Interactions	57
3.2.2	Tau Propagation and Regeneration	58
3.2.3	The TauRunner Program	59
3.3	Detection	60
3.3.1	Detection Methodology	60
3.3.2	The Giant Radio Array for Neutrino Detection (GRAND)	61
3.3.3	The Probe of Extreme Multi-Messenger Astrophysics (POEMMA)	61
3.3.4	Other Observatories	62

4	Earth-Traversing RHN Simulations and their Results	65
4.1	Implementation of the RHN Model	65
4.1.1	The Altered Journey	65
4.1.2	Adapting TauRunner	68
4.1.3	Quantities of Interest	69
4.2	Results	71
4.2.1	Simulation Results	71
4.2.2	Discussion of Small Emergence Angles	71
4.2.3	Discussion of Large Emergence Angles	73
5	Detector Simulations and their Results	75
5.1	Detection Methodology and Effective Area	75
5.2	GRAND Simulations	77
5.2.1	Implementation	77
5.2.2	Results and Discussion	78
5.3	POEMMA Simulations	81
5.3.1	Implementation	81
5.3.2	Results and Discussion	82
5.4	Detector Comparisons	84
5.4.1	Key Differences	84
5.4.2	Outcome	85
6	Final Results and Discussions	87
6.1	Methodology for Probing Parameter Space	87
6.1.1	Utility of Diffuse and Transient Sources	88

6.1.2	Choice of UHE Neutrino Source	89
6.1.3	Strategy and Statistical Approach	91
6.2	Results	91
6.2.1	Key Results and Discussions	91
6.2.2	Sensitivity to Approximations	94
7	Conclusions	97
7.1	Summary	97
7.2	Further Study	98
7.3	Closing Remarks	99
	Bibliography	101

List of Figures

- 2.1 The Feynman vertices available to a Standard Model neutrino of flavour l , often defined as neutral current (NC, left) and charged current (CC, right) interactions respectively 41
- 2.2 Feynman diagrams of the scatterings available in our BSM scenario. Those including a τ are charged current (CC) interactions; the remainder are neutral current (NC) interactions. The BSM right-handed neutrino N is highlighted in red. 49
- 2.3 The decay length of a right-handed neutrino of energy $E = 10$ EeV as a function of its mass m_N in a model with mixing angle θ_{mix} . The diameter of the Earth, $2R_{\text{Earth}}$, is provided for reference. 51
- 3.1 A rough plot of the broken power law $I_N(E) \propto E^{-\gamma}$ described in Refs. [2, 3], with intensity $I_N(E)$ as defined in Ref. [3], provided to illustrate the approximate spectrum of cosmic rays at high energies. The knee, second knee, and ankle features are labelled for reference, in addition to the ultra-high-energy cosmic ray (UHECR) regime. The GZK limit has been applied qualitatively for illustrative purposes; in reality it shows more of a continuous suppression than a discrete cut-off. 54

-
- 3.2 An example track for an Earth-traversing UHE τ neutrino (travelling from bottom left to top right) in the context of the Standard Model. Black solid lines and dotted lines depict the particle propagating as a τ neutrino and charged τ lepton respectively, with the larger dots representing interactions and decays as labelled. The temporary propagation of the particle as a τ before re-converting to a ν_τ constitutes an example of ν_τ regeneration. 59
- 4.1 Example tracks for an Earth-traversing UHE τ neutrino (travelling from bottom left to top right) in the context of the Standard Model (first diagram) and under the influence of our BSM model (second diagram). Black solid lines and dotted lines depict the particle propagating as a τ neutrino and charged τ lepton respectively, with the larger dots representing interactions and decays as labelled. The temporary propagation of the particle as a τ before re-converting to a ν_τ constitutes an example of ν_τ regeneration. In the second diagram, the propagation of the right-handed neutrino N is represented in red. The temporary propagation of the particle as a RHN before reverting to a τ or ν_τ contributes to ν_τ regeneration. 67
- 4.2 A flowchart illustrating the interactions and decays available to a particle in our simulations. Grey items are featured in the base version of `TauRunner`, while red items represent the BSM modifications implemented in our adapted version. Dashed bordering is applied to those particles that, having exited the Earth, may enable detection via an EAS in the atmosphere. 69
- 4.3 A schematic to illustrate the relevant geometry: the emergence angle θ_{em} , the EAS angle θ_{EAS} , and the atmospheric altitude h_{atm} . GRAND (with its incline of α) and the POEMMA satellites are additionally depicted. 70

-
- 4.4 The results of our Earth-traversing UHE neutrino simulations, showing the variation of P_{exit}^i with the emergence angle θ_{em} , for a chosen RHN mass of $m_N = 3$ GeV and various choices of the mixing angle θ_{mix} , simulated for different initial neutrino energies E_ν in the respective plots. Solid lines are for RHNs ($i = N$) and dashed lines are for charged τ leptons ($i = \tau$). 72
- 5.1 The variation of the effective area $\mathcal{A}_{\text{eff}}^i$ calculated from our GRAND simulations with the mixing angle θ_{mix} , for charged τ leptons ($i = \tau$, dashed) and RHNs ($i = N$, solid), for different choices of the initial neutrino energy E_ν . It should be noted for clarity that the dashed black line and dashed light blue line for $E_\nu = 1$ EeV and $E_\nu = 100$ EeV τ leptons respectively are overlapping. 79
- 5.2 The total effective area of POEMMA in our scenario (averaged over energy bins in the range 1–100 EeV) against the mixing angle parameter θ_{mix} , for a chosen geometry of $\theta_{\text{em}} = 70^\circ$, shown for various choices of the RHN mass m_N 83
- 6.1 The neutrino fluence expected from a 221009A-like GRB, as sourced from Ref. [4], rescaled according to the distance D from Earth . . . 90
- 6.2 The sensitivity of the proposed RHN search using POEMMA, considering a transient event similar to GRB 221009A at an example emergence angle of $\theta_{\text{em}} = 60^\circ$, at various distances D . The search is restricted to exit energies of $10 \text{ EeV} \leq E_{\text{exit}} \leq 100 \text{ EeV}$ for the results in the first panel, and to the broader range of $1 \text{ EeV} \leq E_{\text{exit}} \leq 100 \text{ EeV}$ for those in the second panel. The limits from CHARM [5, 6], DELPHI [7], and SHiP [8] are provided for comparison. 93

-
- 6.3 The sensitivity, as depicted in Fig. 6.2, for the case of $D = 50$ kpc with exit energies restricted to $10 \text{ EeV} \leq E_{\text{exit}} \leq 100 \text{ EeV}$, for differing values of the effective opening angle θ_{EAS} (first panel) and the atmospheric altitude h_{atm} (second panel) 95

List of Tables

2.1	The matter content of the Standard Model, where the final column contains the hypercharge Y of each field. The distinction between hypercharge and the electric charge of QED is relevant to the $SU(2)_L$ doublets, where electric charge emerges after the Higgs mechanism as the operator $Q = \frac{1}{2}\sigma_3 + Y$, taking eigenvalues $\pm\frac{1}{2} + Y$, with $(+\frac{1}{2})$ for the field at the top of the doublet and $(-\frac{1}{2})$ for the field at the bottom of the doublet, as arranged in Eqs. (2.1.22) and (2.1.23)	36
2.2	Values of the parameter $L(m_N)$ —that is, the decay length λ_N , calculated for an RHN of energy $E = 1$ EeV in a model with mass m_N and mixing angle $\theta_{\text{mix}} = 10^{-2}$ —for various values of the RHN mass m_N	50
3.1	A list of the UHE neutrino observatories mentioned in this thesis, including the medium observed and signal type detected by each. Bold type denotes those to which our methods are applied in forthcoming chapters.	63

Declaration

The work in this thesis is based on research carried out in the Department of Physics at Durham University. No part of this thesis has been submitted elsewhere for any degree or qualification.

The relevant research was published in the form of Ref. [1]—R. Heighton, L. Heurtier, and M. Spannowsky, *Hunting for neutral leptons with ultra-high-energy neutrinos*, *Phys. Rev. D* **108** (Sep, 2023) 055009—and much of this thesis is based on that publication, including the reproduction of various figures.

Copyright © 2025 Robert Heighton.

The copyright of this thesis rests with the author. No quotation from it should be published without the author's prior written consent and information derived from it should be acknowledged.

No part of this thesis should be used in the training set(s) of any form of 'AI' or machine learning algorithm without the author's prior written consent.

Acknowledgements

The author would like to thank Dr. Lucien Heurtier for his collaboration and academic guidance over the course of the research presented in this thesis, and Professor Michael Spannowsky for his supervision.

I am grateful to my family for their continued support, and to my friends—namely Louise, Adam, Andrew, Joel, Evan, and Jacob—for their company and community throughout the duration of my PhD.

Additional thanks go to my friend and colleague Dr. Mia West for her encouragement, to the community at Josephine Butler College and in the wider Durham sphere, and to the welcoming staff at the Duke of Wellington.

*... let not thy left hand know **what thy right hand doeth***

— Matthew 6:3 (KJV), intended as advice on almsgiving, but
felt by the irreligious author to be serendipitously applicable to
the fundamental physics of neutrinos

*Tyger Tyger, burning bright,
In the forests of the night;
What immortal hand or eye,
Could frame thy fearful symmetry?*

*In what distant deeps or skies.
Burnt the fire of thine eyes?
On what wings dare he aspire?
What the hand, dare seize the fire?*

*And what shoulder, & what art,
Could twist the sinews of thy heart?
And when thy heart began to beat.
What dread hand? & what dread feet?*

*What the hammer? what the chain,
In what furnace was thy brain?
What the anvil? what dread grasp.
Dare its deadly terrors clasp?*

*When the stars threw down their spears
And water'd heaven with their tears:
Did he smile his work to see?
Did he who made the Lamb make thee?*

*Tyger Tyger burning bright,
In the forests of the night:
What immortal hand or eye,
Dare frame thy fearful symmetry?*

Chapter 1

Introduction

The study of high-energy particles arriving at the surface of the Earth from cosmic origins has long been linked to advancements in fundamental physics. In the 1930s–40s, the investigation of cosmic ray tracks in cloud chambers provided extensive contributions to the then-growing particle zoo, including the discoveries of the positron [9], muon [10], pion [11], and kaon [12].

In later decades, focus shifted to collider experiments such as the LHC, testing predictions and extending the boundaries of experimental science with discoveries such as that of the Higgs boson [13], whose confirmed existence was a resounding success for the Standard Model of Particle Physics.

In the meantime, however, the study of astroparticles has by no means dwindled, with major projects on the hunt for cosmic and astrophysical messengers. The Pierre Auger Observatory [14] in Argentina, for example, detects cosmic rays (protons and heavier nuclei) and related phenomena; Super-Kamiokande (Super-K) [15] in Japan and IceCube [16] in Antarctica observe neutrinos over a wide range of energies.

The neutrino, in particular, is a particle of great interest, and is the chosen focus of this thesis.

1.1 Neutrinos and Ultra-High Energies

Observations and measurements of neutrino fluxes of extraterrestrial origin have already illuminated new areas of physics beyond the Standard Model (BSM). The confirmation of neutrino flavour oscillation—and hence the confirmation that neutrinos have mass—at Super-K [17] and the Sudbury Neutrino Observatory [18] won Takaaki Kajita and Arthur B. McDonald the Nobel Prize in Physics in 2015.

In this work, we turn in particular to larger energy scales, to consider neutrinos of ultra-high energy (UHE). Here, we define ultra-high energy as that of around EeV order—that is, approximately 10^{18} eV—and above. Such neutrinos are expected to be produced cosmogenically by the interaction of ultra-high-energy cosmic rays (UHECRs) with the cosmic microwave background, and by transient astrophysical events, as elucidated in forthcoming chapters.

Projects such as Auger [14], IceCube [16], ANITA [19], and ANTARES [20] have pioneered the observation of UHE neutrinos, and the next generation of detectors, including GRAND [21], POEMMA [22], PUEO [23], TAMBO [24], TAROGE-M [25], and Trinity [26], are expected to probe this regime with increased sensitivity, constraining the cosmogenic neutrino flux and opening new avenues of study for high-energy astroparticle physics.

The energies of UHE neutrinos are several orders of magnitude above the centre-of-mass energies achieved at the LHC, and so it is to be hoped that examining this regime could uncover new signals of BSM physics. Such hints may have already arisen, perhaps in the form of the ANITA Anomalous Events (AAEs).

During its flights, the balloon-borne detector ANITA observed two anomalous events [27, 28], each associated with an upward-travelling particle (expected to be a charged τ lepton produced by a τ neutrino, ν_τ) decaying in the atmosphere after traversing a chord of the Earth's interior. The steeply upgoing angles of these events correspond to significant chord lengths, implying that the neutrino in each case had traversed a considerable distance through the planet before emerging to produce the detected

decay. Given the current limits on the neutrino-nucleon interaction cross section, which increases with the neutrino's energy, such a long column of the Earth's matter should be effectively opaque to neutrinos of the EeV-order energies measured, due to scatterings and the energy losses incurred thereby. Such a neutrino could perhaps skim the Earth at a shallow angle, traversing only a short distance through its interior, but at the deeper angles implied it would be highly unlikely to survive the journey with energy of such magnitude.

Analysis showed that a diffuse ν_τ flux, as might be produced isotropically by the cosmos via processes described in more detail in Chapter 3, was not statistically sufficient to realistically produce these events [29], considering current observational constraints on the magnitude of such a flux and assuming SM interactions. Furthermore, IceCube provided constraints [30] to rule out the possibility of a particularly bright transient astrophysical source, and so these events are considered unexplained in the context of the Standard Model.

Various studies [31–34] have proposed BSM explanations for the AAEs, connecting them to—for example—dark matter, axion quark nuggets (a previously-proposed cold dark matter candidate formed from quarks during a QCD phase transition [32, 35]), supersymmetry, and sterile neutrinos. The work in this thesis does not seek to explain the AAEs in particular, but they serve as a more general example of UHE neutrino studies hinting at physics beyond the Standard Model.

1.2 Probing Physics beyond the Standard Model

With a new generation of large-volume UHE neutrino observatories on the horizon, theoretical studies have proposed predictions of the impact of BSM physics on future observations.

Ref. [36], for example, considers the effects of various BSM theories on the neutrino-nucleon and neutrino-electron cross sections, computing sensitivities to the BSM

signals at GRAND, POEMMA, and Trinity. Ref. [34] suggests a sterile neutrino origin for the AAEs, considering an incoming ν_4 that traverses a chord of the Earth and interacts with nucleons to ultimately produce a τ whose subsequent decay would be observed in the atmosphere.

In this work, we consider the scenario of UHE neutrinos incident on the Earth in the context of a BSM model (unlike Refs. [31, 34], where the incoming particles are themselves BSM). In addition to the effects on cross section (as are considered in Ref. [36]) we imagine the production of—and temporary propagation as—BSM particles by UHE neutrinos.

In the Standard Model case, a UHE τ neutrino may, via a charged current interaction with a nucleon in the Earth, produce a charged τ lepton that travels a distance through the Earth before decaying back to a ν_τ , thereby replenishing a previously lost fraction of the neutrino flux through a process generally referred to as ν_τ regeneration. Let us consider a similar effect involving, in place of the τ lepton, some long-lived BSM candidate, produced by a UHE neutrino, that may propagate some distance through the Earth with no or few interactions (due to a small cross section suppressed by the weakness of its mixing with normal matter), before eventually reverting to a ν_τ and thus helping UHE neutrinos survive their Earth-traversing journey.

We choose as our candidate a Majorana right-handed neutrino (RHN) that mixes weakly with the leptons of the Standard Model, and simulate in Python-based programs the journey of a UHE ν_τ through the Earth in the context of this BSM scenario, subsequently simulating detector results and thence probing the parameter space of the model for regions of sensitivity to BSM signals at future large-volume observatories.

1.3 The Structure of this Thesis

Chapter 2 begins with an introduction to the Standard Model of Particle Physics, followed by a discussion of the nature of neutrinos in both theory and experiment,

and concludes with a motion toward BSM physics and the establishment of our RHN model.

Chapter 3 tells the story of an Earth-traversing UHE neutrino from beginning to end, in the unaltered Standard Model case, starting with a discussion of the cosmogenic and astrophysical sources expected to produce UHE neutrinos, detailing the interactions and processes affecting a UHE neutrino as it traverses a chord of the Earth's interior, and concluding with an overview of the detection of such particles at observatories.

In **Chapters 4 and 5**, I present and discuss the results of my Earth-traversing UHE neutrino simulations and detector simulations respectively, analysing how the BSM model and its parameters affect the exit probabilities, energy distributions, and detection probabilities of a UHE neutrino flux at different angles, considering signals at two next-generation observatories of interest: the Giant Radio Array for Neutrino Detection (GRAND), a ground-based array of radio antennae spread over mountainous slopes, and the Probe of Extreme Multi-Messenger Astrophysics (POEMMA), two satellite-borne detectors orbiting at an altitude of 525 km.

Chapter 6 then demonstrates a search through the space of model parameters for statistically significant effects, and presents the final results, followed by some concluding remarks and suggestions for further study in **Chapter 7**.

Chapter 2

The Standard Model and Beyond

2.1 The Standard Model of Particle Physics

The twentieth century saw numerous revolutionary advancements in the field of theoretical physics, as new ideas left behind the classical to explore the relativistic and the quantum. From these developments emerged a reductively elegant, highly predictive, and empirically supported modern theory of particle physics that, despite its unassuming name, remains our best picture of matter at the fundamental level. It is known as the Standard Model.

The Standard Model (SM) is a quantum field theory (QFT) that describes elementary particle species as spacetime-pervading fields whose excitations give rise to the objects we interpret as particles. Some are fermionic (known as matter fields) and others are bosonic (known as force fields or gauge fields), and their mutual interactions underpin particle dynamics, providing a theoretical understanding of three of the four so-called fundamental forces of nature: the strong force, the weak force, and electromagnetism. They are governed by a key defining feature and framework of the Standard Model: gauge symmetries.

2.1.1 The SM Gauge Group and Spontaneous Symmetry Breaking

The Standard Model [37–41] may be summarised by the direct product gauge group

$$SU(3)_C \times SU(2)_L \times U(1)_Y \quad (2.1.1)$$

where each factor is a gauge symmetry under which the emergent physics is invariant. Each corresponds approximately to a fundamental force of nature, excluding only gravity.

The $SU(3)_C$ piece represents the strong interaction that affects quarks and is mediated by the gluon as its gauge boson. The strong sector is described by quantum chromodynamics (QCD) and is labelled with a subscript C for the conserved quantity of colour.

The remaining factors, $SU(2)_L \times U(1)_Y$, are less straightforwardly associated with distinct fundamental forces, together composing the electroweak sector, a unification of the weak force and electromagnetism. The subscript L of $SU(2)_L$ reminds us that only left-handed fermions (i.e. those of left-handed chirality) are affected by the weak interaction, but the subscript Y of $U(1)_Y$ does not directly correspond to electromagnetism, referring instead to the weak hypercharge, an electroweak analogue of electric charge denoted Y . The one-to-one correspondence between symmetries and fundamental forces (and, indeed, the distinction between the electromagnetic force and weak interaction as separate entities) is muddled by the influence of the Higgs boson, a scalar field whose existence was predicted in 1964 [42], and whose eventual discovery in 2012 [13] constituted a decisive victory for the predictive power of the Standard Model and for science as a whole.

The non-vanishing vacuum expectation value of the Higgs field results in spontaneous symmetry breaking (SSB), often illustrated as

$$\mathrm{SU}(2)_L \times \mathrm{U}(1)_Y \rightarrow \mathrm{U}(1)_{\mathrm{EM}} \quad (2.1.2)$$

where we restore the familiar $\mathrm{U}(1)$ symmetry of electromagnetism, described by quantum electrodynamics (QED), with electric charge arising from a combination of weak isospin and hypercharge. The weak force is left with three massive gauge bosons, W^\pm and Z^0 , interacting with charged and neutral left-handed fermions respectively, while one—the photon—remains massless, mediating the electromagnetic force between charged fermions.

2.1.2 The Higgs Mechanism and the Emergence of the Electroweak Gauge Bosons

For future reference within this thesis, it is worthwhile to establish the emergence of the electroweak gauge bosons from SSB in further detail.

We begin with the Higgs Lagrangian

$$\mathcal{L}_H = (D^\mu H)^\dagger (D_\mu H) - V(H) \quad (2.1.3)$$

involving the $\mathrm{SU}(2)_L$ Higgs doublet H and the gauge covariant derivative for the electroweak sector $\mathrm{SU}(2)_L \times \mathrm{U}(1)_Y$, defined as

$$D_\mu := \partial_\mu - i\frac{g}{2}\sigma_j A_\mu^j - i\frac{g'}{2}Y B_\mu \quad (2.1.4)$$

where g is a coupling constant relating weak isospin (reflected in the Pauli matrices σ_j) to the three bosons A_μ^j ($j = 1, 2, 3$), and g' couples the hypercharge Y to the boson B_μ . The strong sector is neglected here for simplicity and clarity.

It is the shape of the Higgs potential

$$V(H) = \mu^2 H^\dagger H + \lambda (H^\dagger H)^2 \quad (2.1.5)$$

with

$$\mu^2 < 0 \quad (2.1.6)$$

$$\lambda > 0 \quad (2.1.7)$$

that causes spontaneous symmetry breaking. The so-called ‘Mexican hat’ potential, named for its resemblance to a sombrero when plotted over the plane defined by the two elements of the Higgs doublet, supplies not a unique minimum but a full circle of minima, from which one point must be ‘chosen’ as the vacuum expectation value $\langle H \rangle$, thus spontaneously breaking the symmetry.

We choose a basis such that

$$\langle H \rangle = \frac{1}{\sqrt{2}} \begin{pmatrix} 0 \\ v \end{pmatrix} \quad (2.1.8)$$

is the vacuum expectation value (VEV) of the Higgs field, where v has been experimentally measured as $v \approx 246$ GeV [43].

Examining the term $(D^\mu H)^\dagger (D_\mu H)$ in the Lagrangian in Eq. (2.1.4), and expanding about the Higgs VEV in Eq. (2.1.8), keeping only the lowest-order terms (that is, terms in v and no orders of the Higgs fields), we obtain

$$\mathcal{L}_{\text{mass}} = \frac{1}{8} \begin{pmatrix} 0 & v \end{pmatrix} (gA^{j\mu}\sigma_j + g'B^\mu)(gA_\mu^j\sigma_j + g'B_\mu) \begin{pmatrix} 0 \\ v \end{pmatrix} \quad (2.1.9)$$

$$= \frac{v^2}{8} [g^2(A_\mu^1)^2 + g^2(A_\mu^2)^2 + (gA_\mu^3 - g'B_\mu)^2] \quad (2.1.10)$$

$$= \frac{g^2 v^2}{4} (W^+)_\mu (W^-)_\mu + \frac{1}{2} \frac{(g^2 + g'^2)v^2}{4} Z^\mu Z_\mu \quad (2.1.11)$$

where in the last line we have chosen the appropriate linear combinations

$$W_\mu^\pm = \frac{1}{\sqrt{2}} (A_\mu^1 \mp iA_\mu^2) \quad (2.1.12)$$

$$Z_\mu = \frac{1}{\sqrt{g^2 + g'^2}} (gA_\mu^3 - g'B_\mu) \quad (2.1.13)$$

$$A_\mu = \frac{1}{\sqrt{g^2 + g'^2}} (gA_\mu^3 + g'B_\mu) \quad (2.1.14)$$

to move into the mass basis and extract the ‘real’ gauge bosons after spontaneous symmetry breaking: the massive electroweak vector bosons W_μ^\pm and Z_μ with masses

$$M_W = \frac{gv}{2} \approx 80.4 \text{ GeV} \quad (2.1.15)$$

$$M_Z = \frac{v\sqrt{g^2 + g'^2}}{2} \approx 91.2 \text{ GeV} \quad (2.1.16)$$

and the massless photon A_μ . The numerical values quoted are those provided in the Particle Data Group’s *Review of Particle Physics* [43].

2.1.3 Yukawa Interactions and Fermion Mass

This Higgs mechanism—or the ABEGHHK’tH mechanism, as named by Higgs in order to acknowledge the contributions of Anderson, Brout, Englert, Guralnik, Hagen, himself, Kibble, and ’t Hooft [44]—is also responsible for giving fermions mass.

In general, we can establish the mass m of a Dirac fermion by introducing to the Lagrangian a term of the form

$$\mathcal{L}_{\text{Dir}} = m\bar{\psi}_L\psi_R + \text{h.c.} \quad (2.1.17)$$

where ψ represents the fermion field, and h.c. henceforth refers to the Hermitian conjugate of the term(s) stated in the expression of a Lagrangian. The left- and right-handed chiral components $\psi_{L,R}$ of the field ψ are the results of applying the projection operators

$$\psi_{L,R} = P_{L,R}\psi \quad (2.1.18)$$

$$= \frac{1}{2} (1 \mp \gamma^5) \psi \quad (2.1.19)$$

where γ^5 is a product of the four Dirac matrices:

$$\gamma^5 = i\gamma^0\gamma^1\gamma^2\gamma^3 \quad (2.1.20)$$

In the Standard Model, however, left-handed and right-handed fields transform differently under the SM gauge group due to the discriminative influence of the weak force, which interacts with only left-handed fermions. As a result, the mass term in Eq. (2.1.17) cannot be gauge invariant, and its straightforward inclusion is prohibited.

We may, on the other hand, include Yukawa interactions between fermions and the Higgs field, described by terms of the form

$$\mathcal{L}_{\text{Yuk}} = -y_d \bar{Q}_L H d_R - y_u \bar{Q}_L \tilde{H} u_R - y_e \bar{L}_L H e_R - y_\nu \bar{L}_L \tilde{H} \nu_R + \text{h.c.} \quad (2.1.21)$$

where

$$Q_L = \begin{pmatrix} u_L \\ d_L \end{pmatrix} \quad (2.1.22)$$

(with hypercharge $Y = \frac{1}{6}$) and

$$L_L = \begin{pmatrix} \nu_L \\ e_L \end{pmatrix} \quad (2.1.23)$$

(with hypercharge $Y = -\frac{1}{2}$) are the left-handed $SU(2)_L$ doublets of the quarks and leptons respectively; u , d , e , and ν are the fermionic fields of the up-type quarks, down-type quarks, charged leptons, and neutrinos respectively; the constants y are

the Yukawa couplings; and H is the $SU(2)_L$ Higgs doublet with its conjugate \tilde{H} , defined as

$$\tilde{H}^a = \epsilon^{ab} H_b^\dagger \quad (2.1.24)$$

for $a, b = 1, 2$.

Where a straightforward Dirac mass term such as that in Eq. (2.1.17) would not be gauge invariant under $SU(2)_L$, the presence of H and \tilde{H} in these terms provides an inversely-transforming $SU(2)_L$ object in each, contracting with the fields to render each term a singlet under the gauge symmetry and hence permissible in the Lagrangian.

After spontaneous symmetry breaking, we can expand these terms around the vacuum expectation value of the Higgs,

$$\langle H \rangle = \frac{1}{\sqrt{2}} \begin{pmatrix} 0 \\ v \end{pmatrix} \quad (2.1.25)$$

and, considering only the terms in v , obtain the following:

$$\mathcal{L}_{\text{Yuk},v} = - \frac{v}{\sqrt{2}} (y_d \bar{d}_L d_R + y_u \bar{u}_L u_R + y_e \bar{e}_L e_R + y_\nu \bar{\nu}_L \nu_R) + \text{h.c.} \quad (2.1.26)$$

We have thus arrived back at mass terms of the form established in Eq. (2.1.17), where each fermion $f = d, u, e, \nu$ now has a mass m_f given by

$$m_f = \frac{y_f v}{\sqrt{2}} \quad (2.1.27)$$

The masses of the fermions thus arise from their interactions with the Higgs field, with each fermion obtaining a mass directly proportional to its Yukawa coupling.

It should be noted that the presence of a Yukawa term for the neutrino in Eqs. (2.1.21) and (2.1.26), which here has been included for completeness, presupposes the exist-

	SU(3) _C	SU(2) _L	U(1) _Y
Q_L	triplet	doublet	$\frac{1}{6}$
L_L	singlet	doublet	$-\frac{1}{2}$
u_R	triplet	singlet	$\frac{2}{3}$
d_R	triplet	singlet	$-\frac{1}{3}$
e_R	singlet	singlet	-1
ν_R	singlet	singlet	0

Table 2.1: The matter content of the Standard Model, where the final column contains the hypercharge Y of each field. The distinction between hypercharge and the electric charge of QED is relevant to the SU(2)_L doublets, where electric charge emerges after the Higgs mechanism as the operator $Q = \frac{1}{2}\sigma_3 + Y$, taking eigenvalues $\pm\frac{1}{2} + Y$, with $(+\frac{1}{2})$ for the field at the top of the doublet and $(-\frac{1}{2})$ for the field at the bottom of the doublet, as arranged in Eqs. (2.1.22) and (2.1.23)

ence of a right-handed neutrino ν_R . This assumption will be explored in due course as we expand upon the physics of neutrinos in Section 2.2.

2.1.4 A Good Theory

In Sections 2.1.1–2.1.2, we have outlined the gauge symmetry framework of the Standard Model and established the theoretical background describing the generation of fermion masses from the Higgs mechanism. A more expansive introduction to the Standard Model (and a useful reference source in the formulation of various parts of this chapter) can be found among the renowned lecture notes of Professor David Tong [41].

For completeness, the matter content of the Standard Model may be summarised with the charges and representations under the gauge group listed in Table 2.1.

By rooting particle dynamics in a mathematically elegant framework of quantum fields and gauge symmetries, the Standard Model is a successful reductionist theory of particle physics. From its base principles, we can derive recipes for constructing Feynman diagrams and computing amplitudes, enabling the calculation of scattering cross sections and other predictions that may be tested with experiment. The eventual discovery of the Higgs boson at the Large Hadron Collider in 2012 [13] constituted a great victory for the Standard Model, consolidating it as our best picture of particle physics to date.

The Standard Model is a successful effective field theory, describing most matter at low energies (of order \sim TeV and below) with comfortable accuracy. It is, however, incomplete.

In subsequent sections, we will explore some of the limitations and failings of the Standard Model, and how the neutrino in particular may pose a pertinent avenue of study. Section 2.2 provides an introduction to neutrino physics, outlining both the nature of the neutrino within the Standard Model and observations that point to physics beyond it. Section 2.3 then extends further into the world of BSM physics, ultimately formulating the model on which the core findings of this thesis are predicated.

2.2 Neutrinos

Having established the context of the Standard Model, we now turn to examine one particle species in particular: the neutrino.

2.2.1 A Brief History

The first hints of the neutrino in scientific study appeared in observations of beta radiation in the early twentieth century. At this time, the process of beta decay was

understood as the transition of some radioactive nucleus A to a daughter nucleus B , via the emission of an electron:

$$A \rightarrow B + e^- \quad (2.2.1)$$

Various experiments (e.g. [45] in 1926) had measured the energy of the emitted electron, and found that it sampled a continuous energy spectrum, as opposed to being fixed for all decays of a particular type. This posed a problem. The momenta of the daughter particles in a two-body decay are determined by conservation of energy and conservation of momentum, and so the electron produced in the decay described in Eq. (2.2.1) would have a fixed energy that, in the centre-of-mass frame of the parent nucleus A , would be straightforwardly calculable given the masses of the nuclei and the electron. In such experiments, this theoretical electron energy was found to constitute merely an upper bound for the observed energy; a variable quantity of energy was missing.

While some (e.g. Niels Bohr [46]) interpreted these results as evidence against the conservation of energy as a rigid law, Wolfgang Pauli postulated in 1930 [47] the existence of a third, unseen decay product that could carry away the missing energy and momentum. Recognising that this light particle would need to be electrically neutral for charge to be conserved, he referred to it as a neutron, a term later reapplied and replaced by Fermi's coining of neutrino.

Inclusion of the neutrino (specifically, in fact, the electron antineutrino $\bar{\nu}_e$) as a decay product transforms Eq. (2.2.1) into

$$A \rightarrow B + e^- + \bar{\nu}_e \quad (2.2.2)$$

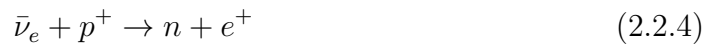
reflecting the now well-understood underlying process of a neutron undergoing beta decay, described at the hadronic level as:

$$n \rightarrow p + e^- + \bar{\nu}_e \quad (2.2.3)$$

where n and p represent the neutron and proton respectively.

The theoretical evidence for the neutrino's existence grew, awaiting experimental validation. The search was—and, to an extent, remains in modern neutrino physics—hindered by the very small cross sections of the weak interactions between neutrinos and other, more familiar particles. Finding neutrinos would require both a large neutrino flux and a large volume of matter in which detectable interactions could take place.

In 1956, experiments by Clyde Cowan and Frederick Reines at the Savannah River nuclear reactor provided conclusive results [48]. In a large volume of water, the vast flux of antineutrinos produced by the reactor interacted via inverse beta decay events (at a rate of a few per hour) with the protons of water molecules to produce detectable positrons:



This work, which won Reines the 1995 Nobel Prize in Physics (unfortunately awarded after Cowan's death), is often referred to as the Cowan-Reines neutrino experiment, and is generally considered the first empirical confirmation of the neutrino's existence.

The general concept of using a vast volume of water to 'catch' neutrinos persisted, and remains a prolific detection strategy to this day. The Super-Kamiokande observatory [15] in Japan uses 50,000 tons of water, surrounded by approximately 13,000 photomultipliers, to observe the Cherenkov radiation emitted by charged particles produced by neutrino interactions, while the IceCube observatory [16] employs a similar methodology with an array of 5,160 digital optical modules distributed throughout a cubic kilometre of ice.

Today, neutrinos are routinely detected in great numbers—enough, in Super-K's case, to image the Sun at night by detecting neutrinos that have traversed the interior of the Earth—and the neutrino has taken its rightful place in the Standard Model, as set out forthwith in Section 2.2.2. The particle's scientific history is far from

over, however, with findings from more recent decades illuminating phenomenology beyond the predictions of the Standard Model, as will be introduced in Section 2.2.3. The historical narrative that has been outlined here is covered in detail and expanded upon in David Griffiths' *Introduction to Elementary Particles* [49] and in the overview provided by Ref. [50].

2.2.2 Neutrinos in the Standard Model

The neutrino features in the Standard Model of Particle Physics as a neutral lepton. The leptonic sector comprises those fermions that are not subject to the influence of the strong force (as are the remaining fermions, quarks) and includes both charged leptons—the electron, e , alongside its successively heavier counterparts the muon, μ , and the tau, τ , all of charge $-1e$, where e is the elementary charge—and neutrinos, all of neutral electric charge. There exist three species of neutrino, known as flavours, corresponding to the three generations of charged lepton: the electron neutrino, ν_e , the μ neutrino, ν_μ , and the τ neutrino, ν_τ . These labels specify the charged lepton with which a given flavour of neutrino interacts; the neutrino produced in the beta decay of Eq. (2.2.3) is of the electron flavour (in particular, an electron antineutrino $\bar{\nu}_e$), as it is produced alongside an electron.

In the context of the Standard Model and the three fundamental forces described therein, neutrinos interact with other particles only via the weak force. In the notation of Feynman diagrams, a neutrino line may be involved in the vertices illustrated in Fig. 2.1, as described (in the relevant example case of the τ neutrino) by the Lagrangian terms

$$-\mathcal{L} \supset \frac{g}{\sqrt{2}} \left(W_\mu^+ \bar{\nu}_\tau \gamma^\mu P_L \tau + \text{h.c.} \right) + \frac{g}{2 \cos \theta_W} Z_\mu \bar{\nu}_\tau \gamma^\mu P_L \nu_\tau \quad (2.2.5)$$

where θ_W is the Weinberg angle, defined such that $\tan \theta_W = g'/g$.

An interaction between a neutrino and other matter (e.g. a nucleon) via the exchange of a boson is often referred to as a neutral current (NC) or charged current (CC)

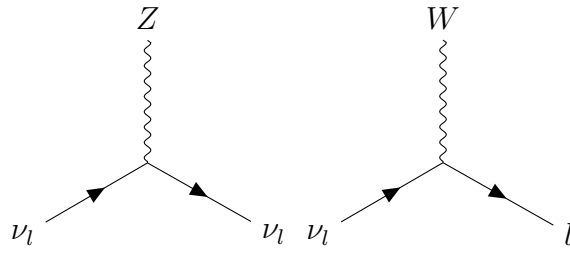


Figure 2.1: The Feynman vertices available to a Standard Model neutrino of flavour l , often defined as neutral current (NC, left) and charged current (CC, right) interactions respectively

interaction, depending on whether the exchanged particle is the neutral Z^0 boson or the charged W^\pm boson.

A consequence of the neutrino's sterility with respect to the other two fundamental forces of the SM is that, due to the selective nature of the weak force, only left-handed neutrinos may appear in the interactions and dynamics of the Standard Model. In a minimal form of the theory, the right-handed neutrino is something of a non-entity, and its traditional inclusion in the SM Lagrangian is primarily by analogy with the other fermions.

Without a right-handed neutrino field, we cannot construct a Yukawa term of the form outlined in Eqs. (2.1.21) and (2.1.26), and so neutrinos cannot gain a mass via the Higgs mechanism, as do the other fermions. The neutrinos of the Standard Model are sometimes considered massless.

2.2.3 Oscillation and Mass

We turn again now to the unfolding history of the neutrino in scientific study. As described in Section 2.2.1, the 1950s saw the confirmation of the neutrino's predicted existence. As early as the 1960–70s, however, a rich new property of neutrinos began to rear its head in experiment.

The Homestake experiment [51], led by Ray Davis Jr., provided the first observations

of solar neutrinos, the neutrinos produced by nuclear fusion in the Sun. The results, however, posed a problem; the flux of electron neutrinos detected was close to one third of that predicted by the calculations of John Bahcall, Davis's collaborator. Other observations (see Ref. [52] for a good review of the history) contributed to a building theme of missing neutrinos, leading to the acknowledgement of the so-called Solar Neutrino Problem: the apparent disappearance of electron neutrinos as they travelled from the Sun to the Earth.

Further studies [17, 18, 53] ultimately led to a solution: neutrino oscillation. As they travel, neutrinos oscillate between flavours; a neutrino originally produced as an electron neutrino ν_e can be detected at its destination as a μ neutrino ν_μ or a τ neutrino ν_τ .

In the theoretical framework of particle physics, neutrino oscillation can be explained by a misalignment between mass eigenstates and flavour eigenstates. Neutrinos can be described by different linear combinations of the three fields present, and the choice of basis that treats the three flavours of neutrino as distinct is not equivalent to the choice of basis that diagonalises the mass matrix and so allows us to describe the 'real' neutrinos that propagate from the Sun to Earth.

The neutrinos detailed so far, which appear in the couplings of Fig. 2.1 and in the interaction terms of the SM Lagrangian, have been the flavour states ν_e , ν_μ , and ν_τ .

Once we have diagonalised the mass matrices in order to work in the mass basis, with mass states ν_1 , ν_2 , and ν_3 , we uncover Lagrangian terms whose currents include a mixing matrix U such that

$$\begin{pmatrix} \nu_e \\ \nu_\mu \\ \nu_\tau \end{pmatrix} = \begin{pmatrix} U_{e1} & U_{e2} & U_{e3} \\ U_{\mu1} & U_{\mu2} & U_{\mu3} \\ U_{\tau1} & U_{\tau2} & U_{\tau3} \end{pmatrix} \begin{pmatrix} \nu_1 \\ \nu_2 \\ \nu_3 \end{pmatrix} \quad (2.2.6)$$

where $\nu_{e,\mu,\tau}$ are the flavour states and $\nu_{1,2,3}$ are the physical mass states.

The matrix U is commonly referred to as the PMNS matrix, after Pontecorvo,

Maki, Nakagawa, and Sakata, the latter three of whom developed the theory of neutrino mixing [54] to explain the oscillations theorised by the former, all before the Homestake experiment had taken place and the Solar Neutrino Problem had arisen in experiment.

The values of the mixing angles underlying the constituent elements of the PMNS matrix are deduced from experiment, and have not yet been derived from any deeper physical principles. Current empirical values [55] are

$$U = \begin{pmatrix} 0.801 \leftrightarrow 0.842 & 0.519 \leftrightarrow 0.580 & 0.142 \leftrightarrow 0.155 \\ 0.252 \leftrightarrow 0.501 & 0.496 \leftrightarrow 0.680 & 0.652 \leftrightarrow 0.756 \\ 0.276 \leftrightarrow 0.518 & 0.485 \leftrightarrow 0.673 & 0.637 \leftrightarrow 0.743 \end{pmatrix} \quad (2.2.7)$$

where each pair of numbers represents a 3σ range of confidence. It may be noted that the PMNS matrix is considerably non-diagonal, and so neutrino oscillation is a significant effect.

From the experimental observation and theoretical foundation of neutrino oscillation, we may deduce that neutrinos have mass. Qualitatively, it is apparent from quantum mechanics that a misalignment between nominal states and energy (i.e. neutrino mass) eigenstates should result in a relative phase

$$e^{-i\Delta Et} \quad (2.2.8)$$

governing the time-evolution of the superposition of states, where ΔE is the energy difference between the two energy states. In the case of high-energy neutrinos, it can be derived from the relativistic dispersion relation that

$$\Delta E = \frac{\Delta m^2}{2E} \quad (2.2.9)$$

with a square mass difference

$$\Delta m^2 = m_2^2 - m_1^2 \quad (2.2.10)$$

for the two states being considered. Assuming a distance travelled of $L = t$ for a relativistic neutrino, there is hence a relative phase

$$\exp\left(\frac{-i\Delta m^2 L}{2E}\right) \quad (2.2.11)$$

causing the probability of the neutrino having a given flavour at detection to oscillate along its path through space. Oscillatory length scales thus depend on the mass differences Δm^2 between the three generations of neutrino, ν_1 , ν_2 , and ν_3 , as formulated in the mass basis, and the strength of the effect of oscillation is tuned by the mixing angles that appear in the PMNS matrix.

This more recent understanding of neutrinos is at odds with the previously-described postulation of massless neutrinos in the Standard Model, which results from the absence of an interacting right-handed neutrino. Both the massive nature of neutrinos and the need to turn to experiment to determine the constituent values of the PMNS matrix point us in the direction of physics beyond the Standard Model (BSM).

2.3 Beyond the Standard Model

2.3.1 Missing Pieces

The Standard Model, despite its success and efficacy, leaves various phenomena unexplained.

In terms of the so-called fundamental forces, for example, the Standard Model provides theoretical framework for three, while the fourth—gravity—eludes its scope. Theories of quantum gravity have attempted to unify general relativity with the quantum, but none so far have gained scientific consensus. Similarly, the Standard Model has yet to provide an agreed-upon candidate for the identity of dark matter. From a theoretical perspective, there are further issues with the Standard Model, such as the hierarchy problem and the abundance of free parameters in the theory.

The latter includes the PMNS matrix described in the previous section, whose elements are dependent on mixing angles that have been constrained experimentally, but, as of yet, cannot be derived from base principles.

With regard to neutrinos, the Standard Model does not explain the neutrino masses evidenced by observations of oscillation. Even with the inclusion of a right-handed neutrino—and thus a Dirac mass arising from a Yukawa interaction with the Higgs, analogously to Eqs. (2.1.21)–(2.1.27)—new theoretical problems arise: the very small masses of neutrinos, currently bounded by experimental results and cosmological constraints (as discussed more deeply and comprehensively in Chapters 14 and 26 of the Particle Data Group’s *Review of Particle Physics* [43], but with an example of

$$m_{\nu_e} < 0.8 \text{ eV} \quad (2.3.1)$$

from KATRIN [56]), would imply Yukawa couplings approximately 10^6 times smaller than that of the electron, and this vast difference in magnitude between the Yukawa couplings of neutrinos and the Yukawa couplings of other fermions would be yet another unexplained and seemingly arbitrary feature of the model.

It is clear that the phenomenology of neutrinos relates to unknown physics *beyond the Standard Model* (BSM).

2.3.2 The Right-Handed Neutrino and Majorana Mass

As discussed, we may include a right-handed neutrino ν_R in our theory, allowing the construction of a Yukawa term

$$\mathcal{L}_{\text{Yuk}} \supset -y_\nu \bar{L}_L \tilde{H} \nu_R + \text{h.c.} \quad (2.3.2)$$

that, once the Higgs field has obtained a non-zero vacuum expectation value v , gives rise to a Dirac mass

$$m = \frac{y_\nu v}{\sqrt{2}} \quad (2.3.3)$$

as in Eq. (2.1.27).

The nature of the right-handed neutrino as a singlet of the Standard Model gauge group allows us to additionally introduce a Majorana mass term of the form

$$\mathcal{L}_{\text{Maj}} = \frac{1}{2} M \bar{\nu}_R^c \nu_R + \text{h.c.} \quad (2.3.4)$$

where M is a Majorana mass. This models the right-handed neutrino as a Majorana fermion that is its own antiparticle.

Simultaneously including both a Yukawa interaction and a Majorana mass term results in a combined mass term of the form

$$\mathcal{L}_{\text{mass}} = \frac{1}{2} \begin{pmatrix} \bar{\nu}_L & \bar{\nu}_R^c \end{pmatrix} \begin{pmatrix} 0 & m \\ m & M \end{pmatrix} \begin{pmatrix} \nu_L \\ \nu_R \end{pmatrix} + \text{h.c.} \quad (2.3.5)$$

where the off-diagonal elements of the mass matrix have arisen from cross terms relating ν_L and ν_R , and thus sum to the Dirac mass m , while the non-zero diagonal term arises from the right-handed neutrino's Majorana term, and thus equates to its Majorana mass M .

When we diagonalise this matrix to enter the neutrino mass basis, its two eigenvalues become the masses of the neutrino's physical states, given by

$$m_{N,\nu} = \frac{1}{2} \left| M \pm \sqrt{M^2 + 4m^2} \right| \quad (2.3.6)$$

If we choose $M \gg m$, such that the right-handed neutrino's Majorana mass is significantly larger than the neutrino's Dirac mass, we obtain

$$m_N \approx M \quad (2.3.7)$$

and

$$m_\nu \approx \frac{m^2}{M} \quad (2.3.8)$$

In this limit, we may consider the physical state of mass m_N to be approximately the right-handed neutrino, with a mass close to the Majorana mass M , and the physical state of mass m_ν to be approximately the left-handed neutrino.

This formulation is often described as a seesaw mechanism [57, 58], named for how the mass of the mostly left-handed neutrino state can be made arbitrarily small as the mass of the right-handed neutrino (or, more specifically, the ratio M/m) is made arbitrarily large. The existence of a sterile or mostly sterile right-handed neutrino as a Majorana fermion could, via this seesaw mechanism, constitute the origin of the active left-handed neutrino's mass, thus explaining the apparent non-zero masses of observed neutrinos and hence such phenomena as neutrino oscillation.

In particular, such a seesaw mechanism would also help to justify the very small masses of neutrinos, currently estimated at orders of magnitude less than that of the electron. Even with a more natural size for the neutrino's Yukawa coupling—that is, one more comparable to those of other fermions—a sufficiently large value of M would result in neutrino masses below the upper bound established by experiment. We are thus able to metaphorically seesaw mass between the two forms of neutrino, allowing us to tune the theory as appropriate.

2.4 The Model

For the remainder of this thesis, we consider a minimal extension of the SM leptonic sector including the usual three generations of left-handed $SU(2)_L$ doublets with the addition of a right-handed neutrino N : a Majorana fermion, constituting a singlet in the SM gauge group, that mixes with its active left-handed counterpart. We consider a relatively simple scenario where N mixes exclusively with the active τ

neutrino, ν_τ , as governed by a mixing angle θ_{mix} , a variable parameter of this BSM model alongside the right-handed neutrino's mass m_N .

This mixing may be summarised by the addition of the following terms to the Lagrangian:

$$\begin{aligned}
 -\mathcal{L} \supset & -\frac{m_N}{2}\bar{N}^c N + \frac{g}{\sqrt{2}}\sin\theta_{\text{mix}}W_\mu^+\bar{N}^c\gamma^\mu P_L\tau \\
 & + \frac{g}{2\cos\theta_w}\sin\theta_{\text{mix}}Z_\mu\bar{N}^c\gamma^\mu P_L\nu_\tau + \text{h.c.}
 \end{aligned} \tag{2.4.1}$$

2.4.1 Scatterings

Scatterings between the right-handed neutrino (RHN) N and ordinary matter are inherited from the Standard Model scatterings illustrated in Fig. 2.1, and can be neutral current (NC) or charged current (CC) interactions. The full array of available scatterings that may occur between a τ neutrino ν_τ or right-handed neutrino N and a nucleon in the Earth is provided in Fig. 2.2.

The matrix elements of such interactions gain a factor of $\sin^n(\theta_{\text{mix}})$ where n right-handed neutrinos are involved, and so their cross sections gain a factor of $\sin^{2n}(\theta_{\text{mix}})$. On statistical grounds, we may neglect the last interaction in Fig. 2.2, involving two instances of N , as its cross section would gain a factor of $\sin^4(\theta_{\text{mix}})$, rendering such a scattering very rare in the context of the sample sizes and values of θ_{mix} we investigate.

Assuming the Standard Model cross sections σ_{NC} and σ_{CC} for NC and CC interactions between a left-handed neutrino and a nucleon in the Earth, the cross sections of the ‘mixing NC’ interaction (involving one ν_τ and one N) and ‘mixing CC’ interaction (involving one N and one τ) scale with the mixing angle as follows:

$$\sigma_{\text{NC,mix}} = \sigma_{\text{NC}}\sin^2(\theta_{\text{mix}}) \tag{2.4.2}$$

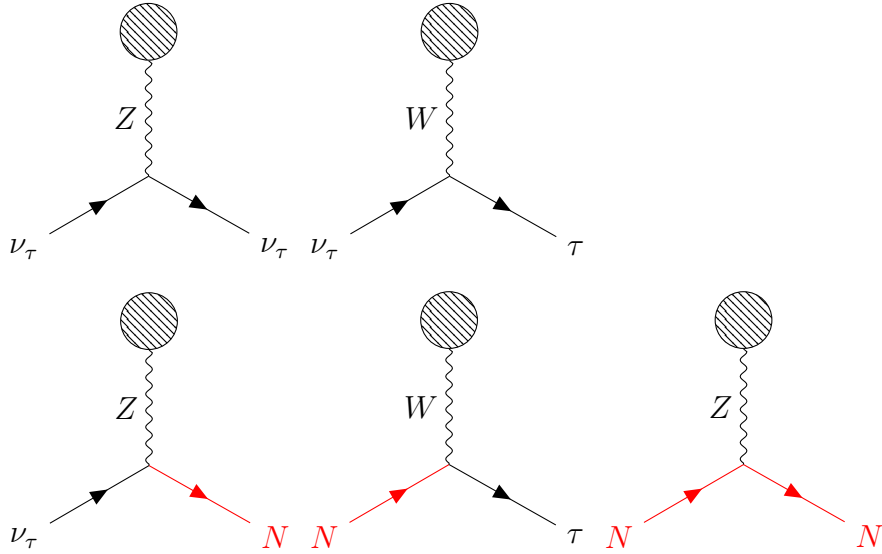


Figure 2.2: Feynman diagrams of the scatterings available in our BSM scenario. Those including a τ are charged current (CC) interactions; the remainder are neutral current (NC) interactions. The BSM right-handed neutrino N is highlighted in red.

$$\sigma_{\text{CC,mix}} = \sigma_{\text{CC}} \sin^2(\theta_{\text{mix}}) \quad (2.4.3)$$

2.4.2 Decays

Depending on the chosen value of the mass parameter m_N , the heavy right-handed neutrino N has access to various two- and three-body decay channels. The comprehensive list used in our simulations was sourced from Appendix C of Ref. [59].

At ultra-high energies, where $E \gg m_N$, the right-handed neutrino is highly boosted, and so its decay length λ_N scales linearly with its energy E , and may be parametrised to illustrate its proportionality as

$$\lambda_N(E; m_N, \theta_{\text{mix}}) \approx \left(\frac{E}{\text{EeV}} \right) \left(\frac{\theta_{\text{mix}}}{0.01} \right)^{-2} L(m_N), \quad (2.4.4)$$

where $L(m_N)$ is its decay length at $E = 1$ EeV in a model with a mixing angle of $\theta_{\text{mix}} = 10^{-2}$. Some example values of $L(m_N)$ at various values of the RHN mass are supplied in Table 2.2.

m_N [GeV]	$L(m_N)$ [km]
3.0	1.10×10^4
5.0	523.
6.0	190.
7.0	79.8
8.0	37.2
14.0	1.41

Table 2.2: Values of the parameter $L(m_N)$ —that is, the decay length λ_N , calculated for an RHN of energy $E = 1$ EeV in a model with mass m_N and mixing angle $\theta_{\text{mix}} = 10^{-2}$ —for various values of the RHN mass m_N

Fig. 2.3 depicts the decay length λ_N as a function of the mass parameter m_N for various values of the mixing angle θ_{mix} , at a chosen energy of $E = 10$ EeV. The scale of the Earth’s diameter is also depicted for comparison, and it is clear that, for the range of mixing angles chosen and the incoming energy considered, the right-handed neutrinos whose decay length is comparable to the scale of the Earth’s diameter—and whose existence may thus aid ultra-high-energy (UHE) neutrinos in their propagation over large distances in the Earth—have masses of $\mathcal{O}(1\text{--}10)$ GeV. This is the approximate region of our search in parameter space.

It should be noted that the decay length parametrised in Eq. (2.4.4) and plotted in Fig. 2.3 is an expectation value. The actual distance the RHN travels before decay is probabilistic, described by an exponential distribution with a mean of λ_N and a variance of λ_N^2 .

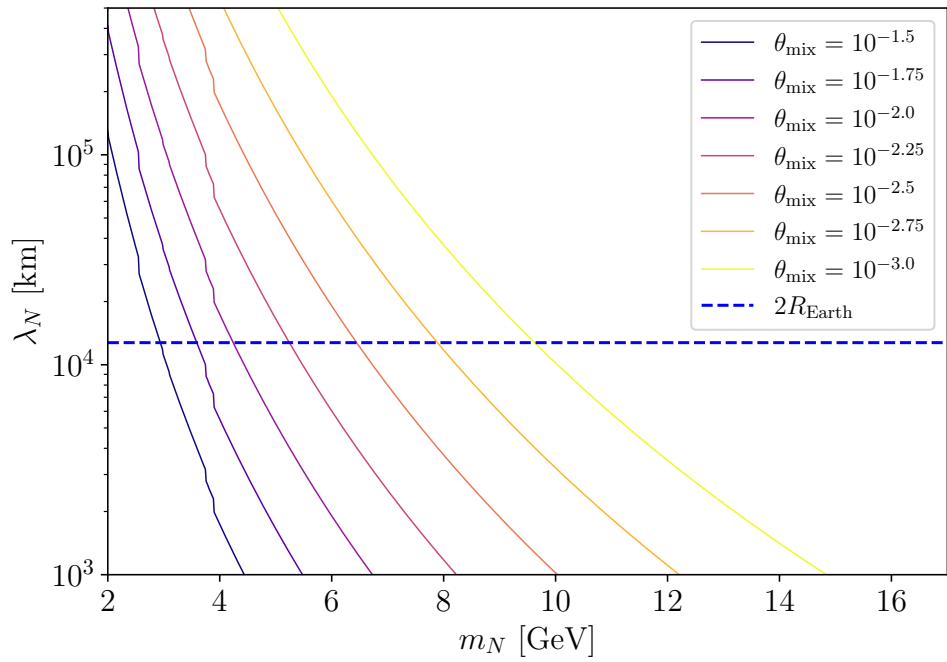


Figure 2.3: The decay length of a right-handed neutrino of energy $E = 10$ EeV as a function of its mass m_N in a model with mixing angle θ_{mix} . The diameter of the Earth, $2R_{\text{Earth}}$, is provided for reference.

Chapter 3

UHE Neutrinos: A Journey through the Earth

In the work presented within this thesis, we consider the effects of the BSM physics discussed on the observation and measurement of ultra-high-energy (UHE) neutrinos that have traversed distances of the Earth's interior.

We must therefore establish: firstly, the sources in the Universe from which we might expect UHE neutrinos to propagate and arrive at the Earth; secondly, the processes that affect a UHE neutrino as it makes its Earth-traversing journey; and, thirdly, detection methodologies and some relevant experimental projects capable of detecting a UHE neutrino flux below the horizon.

3.1 Sources

In the consideration of the sources of UHE neutrinos available for study, it is useful to make a distinction between cosmogenic neutrinos—that is, those originating throughout the Universe as a product of UHE cosmic rays, expected to be observed as an diffuse, isotropic, and approximately constant flux—and the neutrinos produced in transient emissions by specific, localised astrophysical events.

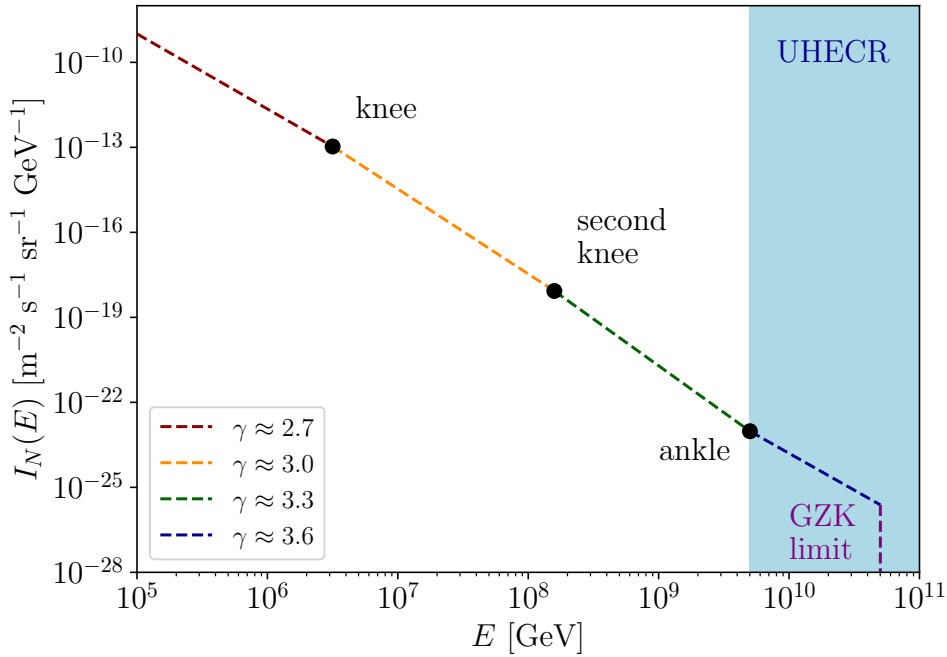


Figure 3.1: A rough plot of the broken power law $I_N(E) \propto E^{-\gamma}$ described in Refs. [2,3], with intensity $I_N(E)$ as defined in Ref. [3], provided to illustrate the approximate spectrum of cosmic rays at high energies. The knee, second knee, and ankle features are labelled for reference, in addition to the ultra-high-energy cosmic ray (UHECR) regime. The GZK limit has been applied qualitatively for illustrative purposes; in reality it shows more of a continuous suppression than a discrete cut-off.

3.1.1 Cosmogenic Neutrinos

One likely source of UHE neutrinos is a cosmogenic flux, predicted to originate at these energies from ultra-high-energy cosmic rays (UHECRs).

Cosmic rays (CRs) are protons and heavier nuclei propagating through the Universe at relativistic speeds. Their energies are distributed over a wide spectrum described by a broken power law illustrated in Fig. 3.1, and those beyond the so-called ankle of this distribution, with energies upward of EeV order, are considered to have ultra-high energy and are referred to as UHECRs.

At energies around $E_{\text{GZK}} \approx 50$ EeV, cosmic ray protons interact resonantly with the cosmic microwave background (CMB), via processes such as

$$p + \gamma \rightarrow \Delta(1232) \rightarrow n + \pi^+ \quad (3.1.1)$$

where $\Delta(1232)$ denotes a family of short-lived baryons (of mass $m_\Delta \approx 1232$ MeV) produced at this resonance. Additionally, heavier cosmic ray nuclei undergo photo-disintegration at such energies.

As a result of these processes, the propagation of such energetic UHECRs is inhibited, and we expect to see a cut-off in the energy spectrum. This so-called Greisen-Zatsepin-Kuzmin limit, named for those who first predicted it [60, 61], has been identified in experiment [62, 63].

The relevance of the GZK cut-off to the study of high-energy neutrinos arises from the products of these photo-hadronic interactions. The pion produced in Eq. (3.1.1), for example, may undergo a decay sequence such as

$$\pi^+ \rightarrow \mu^+ + \nu_\mu \quad (3.1.2)$$

$$\mu^+ \rightarrow e^+ + \nu_e + \bar{\nu}_\mu \quad (3.1.3)$$

and thus prolifically produce neutrinos. The GZK cut-off is hence a source of UHE neutrinos in the cosmos. It should be noted that the flavour of the neutrinos produced in Eqs. (3.1.2)–(3.1.3) is largely irrelevant to the flavour distribution of those that reach the Earth, as neutrino oscillation over the cosmic distances travelled results in an approximately even distribution between the three flavours [64].

Ref. [2] provides a good review of cosmogenic neutrinos and the processes described here.

While convincingly predicted, the GZK flux of UHE neutrinos originating from these processes remains undetected experimentally. A diffuse background of UHE neutrinos has been constrained by the results of observatories such as ANITA [65], IceCube [66], and Auger [67].

3.1.2 Transient Astrophysical Sources

Alternatively, we may look to astrophysical events for our source of ultra-high-energy neutrinos. These can be expected to produce transient emissions over short periods of time (from minutes to months) at localised positions in the sky, as opposed to the approximately constant and isotropic flux predicted for cosmogenic neutrinos.

Sources of this type may include superluminous supernovae (SLSNe), blazar flares, tidal disruption events (TDEs), magnetars, gamma ray bursts (GRBs), and mergers involving neutron stars or black holes [68]. In general, events involving the rapid outflow of material can accelerate protons to high energies at which they undergo photo-hadronic interactions with the CMB like that outlined in Eq. (3.1.1), or—in scenarios involving acceleration through a strong magnetic field—the analogous pB process [69], where the relativistic protons may produce pions and other hadrons as a form of synchrotron radiation via similar resonances.

From an event such as these, involving the rapid ejection of material and sufficient acceleration of protons, we may expect a transient flux of UHE neutrinos.

In the past decade, the advent of gravitational wave (GW) observation [70] has opened a new channel for observing such events. The ability of neutrino observatories to follow up on ongoing astrophysical transients initially detected via electromagnetic or GW channels, and to thence constrain the neutrino fluxes produced by these cosmic accelerators [71, 72], heralds a new era of multi-messenger astronomy.

3.2 In the Earth

We now consider a flux of UHE neutrinos (such as those produced by the sources above) incident on the Earth's surface, and explore the interactions and processes that affect such a neutrino, in the Standard Model case, as it traverses the Earth's interior.

For the purposes of discussing and simulating this scenario, it is helpful to interpret scatterings and decays (the CC interaction, for example, where a τ neutrino ν_τ scatters with a nucleon and the outgoing particle is a charged τ lepton) as transformations of the same particle converting between different species as it follows a linear track through the material of the Earth (meaning that the aforementioned CC example is interpreted as the neutrino ‘becoming’ a charged τ lepton). At ultra-high energies, these particles are so greatly boosted that angular deviations due to scatterings can be neglected, and over the course of its journey through the Earth a given neutrino follows a particular linear path fully determined by the geometry of its angle of incidence and the point on the Earth’s surface at which it entered.

3.2.1 Neutrino-Nucleon Interactions

In the Standard Model case, UHE neutrinos incident on the Earth are likely to interact with nucleons, and may do so via neutral current (NC) or charged current (CC) interactions, corresponding to the two Standard Model diagrams (i.e. those without the red-highlighted right-handed neutrino N) in Fig. 2.2.

In the NC case, a neutrino will lose energy but remain a neutrino, and will likely go on to undergo further scatterings (NC and CC). In the CC case, the neutrino will both lose energy and convert to a charged lepton. In this work, we primarily investigate τ neutrinos, ν_τ , and so the particle produced in a CC interaction is specifically a τ lepton.

The neutrino-nucleon scattering cross sections of these interactions are dominated at high energies by deep inelastic scattering (DIS) processes [73, 74], and, in the UHE regime, scale with the neutrino energy E_ν as approximated by the power laws

$$\sigma_{\text{NC}} \approx (2.31 \times 10^{-36} \text{ cm}^2) \left(\frac{E_\nu}{\text{GeV}} \right)^\alpha \quad (3.2.1)$$

$$\sigma_{\text{CC}} \approx (5.53 \times 10^{-36} \text{ cm}^2) \left(\frac{E_\nu}{\text{GeV}} \right)^\alpha \quad (3.2.2)$$

where the index $\alpha \approx 0.363$ [73], and so the Earth becomes more opaque to the neutrino flux at higher energies.

Neutrino-electron interactions are subdominant at such energies [73] and are neglected here.

3.2.2 Tau Propagation and Regeneration

The charged τ lepton produced by a CC interaction will continue to propagate through the Earth, undergoing various energy losses via effects such as bremsstrahlung and photonuclear interactions [75], and will likely eventually decay, producing a τ neutrino. The additional decay products comprise a pair of leptons (one charged and one neutrino) of a lighter flavour; these are neglected, as neutrinos and charged leptons of lighter flavours cannot regenerate τ neutrinos through their interactions and decays within the model simulated.

The combination of CC interactions and τ decays gives rise to an emergent effect known as ν_τ regeneration or τ regeneration, whereby a τ neutrino initially scatters with a nucleon and converts to a τ via a CC interaction, and later, after propagating some distance, subsequently decays to revert to a τ neutrino (of lesser energy than that with which it began). Some of the ν_τ flux lost due to CC interactions is thus restored or regenerated. The process of ν_τ regeneration significantly impacts the flux and energy spectrum of Earth-traversing UHE neutrinos [76].

The general principle of a regenerative effect (whereby an UHE neutrino may convert to and temporarily propagate as a different particle species before reverting to a neutrino), and the significance such an effect can have on the neutrino flux and energy spectrum detected, is a core motivation in this work. Given that, in the SM case, ν_τ regeneration is such a dominant process in allowing UHE neutrinos at deeper emergence angles to survive and exit the Earth (see Fig. 8 of Ref. [76]), it is reasonable to imagine that BSM physics involving long-lived particles that could propagate over distances comparable to the τ decay length would also play an

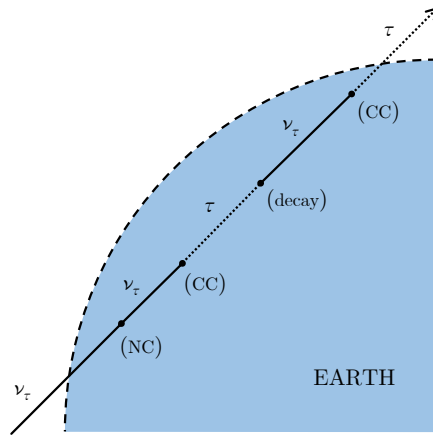


Figure 3.2: An example track for an Earth-traversing UHE τ neutrino (travelling from bottom left to top right) in the context of the Standard Model. Black solid lines and dotted lines depict the particle propagating as a τ neutrino and charged τ lepton respectively, with the larger dots representing interactions and decays as labelled. The temporary propagation of the particle as a τ before re-converting to a ν_τ constitutes an example of ν_τ regeneration.

important role.

In this study, we choose the RHN as our candidate for an intermediate particle through which a UHE neutrino traversing the Earth could regenerate. In this BSM scenario, large-volume detectors measuring the flux of Earth-traversing UHE neutrinos would thus become ideal observatories in the search for this new physics and the constraining of its parameters.

An example track is provided in Fig. 3.2 to qualitatively illustrate the processes affecting an Earth-traversing UHE ν_τ . For a more elaborate review and analysis of Earth-traversing τ neutrinos, see Ref. [76], and for a wider review on τ neutrinos in experiment and simulation, see Ref. [77].

3.2.3 The TauRunner Program

The Python-based program TauRunner [78] was developed to simulate the behaviour of UHE τ neutrinos as they traverse chord lengths of the Earth.

Using Monte Carlo methods to determine instances of scatterings and decays and the involved energy losses, **TauRunner** tracks a given ν_τ along a path determined by geometric inputs, modelling the density of the Earth's material with the Preliminary Reference Earth Model (PREM) [79]. The inclusion of charged τ lepton propagation and decay, as simulated with the **PROPOSAL** package [75], results in the emergent effect of ν_τ regeneration. For a chosen number of τ neutrinos ν_τ of energy E_ν (or with energies sampled from a specified spectrum) traversing the Earth at a specified angle, **TauRunner** outputs a list of Earth-exiting particles and their final energies.

In this work, we use **TauRunner** as a base for our simulations, adapting it to include the right-handed neutrino N discussed in Section 2.4 and its behaviour.

3.3 Detection

Having explored the possible sources of UHE neutrinos and the processes they undergo as they traverse the Earth, we now consider some of the methods and observatories available for their detection.

3.3.1 Detection Methodology

The general detection principle we consider relies on UHE neutrinos undergoing charged current (CC) interactions within the Earth and thus producing a flux of charged τ leptons exiting the surface. The decay of a τ in the atmosphere triggers a chain of reactions that results in a cascade of vast numbers of particles, known as an extensive air shower (EAS).

Importantly, many of the particles in an EAS are electrically charged. The geomagnetic field of the Earth causes a dispersion effect, separating these charged particles into concentrations of positive and negative charge. The resulting time-varying electric current, propagating in the geomagnetic field, induces an emission of electromagnetic radiation in the radio range. This radio emission may be detected

and measured by the radio antennae of a detector such as GRAND [21]. From the observed statistics of the EAS, it is possible to reconstruct knowledge of the primary particle, including its identity, energy, and angle of origin [80].

Such showers also produce Cherenkov emissions, similarly observable by detectors such as POEMMA [22].

While the τ constitutes the detectable particle in the SM case, the BSM model considered would also provide a detection candidate in the form of right-handed neutrino N . As described in Section 2.4.2, N has numerous and varied available decay paths, and its decay in the atmosphere would similarly produce an extensive air shower and result in the reception of a radio emission.

3.3.2 The Giant Radio Array for Neutrino Detection (GRAND)

The Giant Radio Array for Neutrino Detection (GRAND) [21] is a planned observatory for detecting UHE cosmic rays and neutrinos, constituting an array of radio antennae spread over mountainous slopes. These antennae are expected to receive the radio emissions of extensive air showers (EASs) that result from τ (and, in our BSM scenario, RHN) decays.

The planned first iteration is GRAND10k, comprising 10,000 antennae over an area of 10,000 km². Later, in the 2030s, the project expects to develop GRAND200k, composed of 20 independent sub-arrays at separate geographical locations. GRAND10k will be included as one such sub-array, with the others replicating it.

3.3.3 The Probe of Extreme Multi-Messenger Astrophysics (POEMMA)

The Probe of Extreme Multi-Messenger Astrophysics (POEMMA) [22] will comprise two satellites orbiting the Earth at an altitude of 525 km. Unlike ground-based

detectors like GRAND, POEMMA will observe the atmosphere from above, using two possible configurations: the stereo mode, detecting air fluorescence, and the limb mode, detecting the Cherenkov radiation produced by upward-moving extensive air showers.

POEMMA is expected to be effective at target-of-opportunity (ToO) observations [81], as each spacecraft can be quickly reoriented (a 90° change in 500s). This capability for rapid repointing, together with the satellites' high orbital speed, allows POEMMA to promptly follow up on transient sources such as those described in Section 3.1.2, once alerted.

3.3.4 Other Observatories

For reference, Table 3.1 presents a gathered list of the UHE neutrino detectors mentioned in this thesis. A more comprehensive list of next-generation detectors can be found in Table 1 of Ref. [36].

<i>Observatory</i>	<i>Setting</i>	<i>Medium</i>	<i>Technique</i>	<i>Generation</i>
ANITA [19]	balloon	ice	Askaryan	previous
ANTARES [20]	undersea	water	Cherenkov	previous
Auger [14]	ground	water atmosphere	Cherenkov fluorescence	previous
IceCube [16]	in ice	ice	Askaryan	previous
GRAND [21]	mountainside	atmosphere	radio	next-gen.
POEMMA [22]	satellite	atmosphere	fluorescence Cherenkov	next-gen.
PUEO [23]	balloon	atmosphere ice	radio Askaryan	next-gen.
TAMBO [24]	mountainside	atm. and water	Cherenkov	next-gen.
TAROGÉ-M [25]	mountaintop	atmosphere	radio	next-gen.
Trinity [26]	mountaintop	atmosphere	Cherenkov	next-gen.

Table 3.1: A list of the UHE neutrino observatories mentioned in this thesis, including the medium observed and signal type detected by each. Bold type denotes those to which our methods are applied in forthcoming chapters.

Chapter 4

Earth-Traversing RHN

Simulations and their Results

In Chapter 2, we explored the Standard Model, the neutrino in theory and experiment, and a particular BSM extension involving the right-handed neutrino (RHN) N . Chapter 3 outlined the journey of a UHE neutrino through the matter of the Earth in the context of the Standard Model, and described its simulation.

We now combine these avenues of study in order to consider the influence of the RHN on a UHE neutrino's journey through the Earth, and simulate such a scenario.

4.1 Implementation of the RHN Model

4.1.1 The Altered Journey

We now consider the propagation of ultra-high-energy neutrinos in the Earth under the influence of the BSM model described in Section 2.4.

In addition to the usual NC and CC interaction possibilities, a left-handed neutrino traversing the Earth may now additionally undergo a *mixing* NC interaction, corresponding to the first BSM diagram in Fig. 2.2. This is largely analogous to

the Standard Model equivalent, excepting that where the SM case had the particle remain a left-handed neutrino, ν_τ , the outgoing particle of the mixing interaction is the right-handed neutrino N . Relative to that of the NC interaction, the cross section of the mixing NC interaction is suppressed by a factor of $\sin^2 \theta_{\text{mix}}$ as expressed in Eq. (2.4.2).

The right-handed neutrino produced by such a scattering continues to propagate through the Earth. Like its left-handed counterpart, it may scatter with a nucleon via two possible interactions: a mixing NC interaction whereby it reverts to a ν_τ , and a mixing CC interaction whereby it becomes a charged τ lepton (which propagates and ultimately decays back to a ν_τ as in the SM case). The cross sections of both interactions are similarly suppressed by a factor of $\sin^2 \theta_{\text{mix}}$, corresponding to the first two BSM diagrams in Fig. 2.2.

As discussed, N may undergo a doubly-mixing NC interaction whereby it remains a right-handed neutrino, corresponding to the final BSM diagram in Fig. 2.2, but the cross section of such scattering is suppressed by a factor of $\sin^4 \theta_{\text{mix}}$, and is therefore neglected in our simulation on statistical grounds.

Also available to the right-handed neutrino, and generally dominating over the scatterings in our findings, is RHN decay, as outlined in Section 2.4.2. The decay width is strongly dependent on the RHN mass m_N , with terms in m_N^3 and m_N^5 , and with larger masses opening up numerous new hadronic decay channels. RHN decay produces τ neutrinos and charged τ leptons that propagate onward within the Earth, behaving as before. A comparison may be drawn between the production and subsequent decay of an RHN and the SM process of τ regeneration.

An example track is provided in Fig. 4.1 to qualitatively illustrate the processes affecting an Earth-traversing UHE ν_τ in the SM case and BSM case respectively.

In the SM case, a single initial ν_τ incident on the Earth may be regarded (and hence simulated) consistently as a single particle, undergoing interactions and converting between ν_τ and τ (while daughter products of lighter leptonic flavours are neglected),

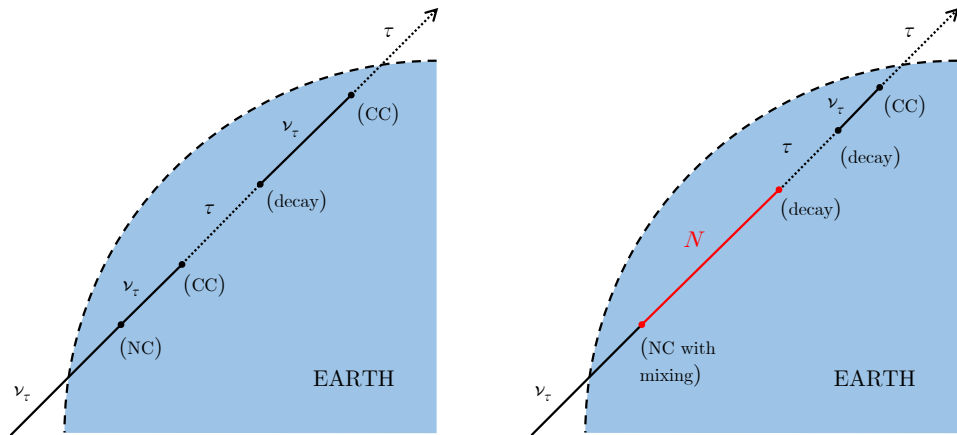


Figure 4.1: Example tracks for an Earth-traversing UHE τ neutrino (travelling from bottom left to top right) in the context of the Standard Model (first diagram) and under the influence of our BSM model (second diagram). Black solid lines and dotted lines depict the particle propagating as a τ neutrino and charged τ lepton respectively, with the larger dots representing interactions and decays as labelled. The temporary propagation of the particle as a τ before re-converting to a ν_τ constitutes an example of ν_τ regeneration.

In the second diagram, the propagation of the right-handed neutrino N is represented in red. The temporary propagation of the particle as a RHN before reverting to a τ or ν_τ contributes to ν_τ regeneration.

but remaining one particle ‘instance’ and resulting in at most one ν_τ or τ exiting the Earth. In the RHN case, however, some RHN decay channels produce multiple instances of the relevant particles. This includes, for example, the decay

$$N \rightarrow \nu_\tau \tau^+ \tau^-, \quad (4.1.1)$$

with a branching ratio of 16–22% for an RHN with mass 4–16 GeV, as calculated from the aforementioned list in Appendix C of Ref. [59]. It is thus necessary, in the context of our BSM model, to account for the proliferation of a single particle instance into multiple; the production and subsequent decay of a right-handed neutrino may result in two or more detectable particles stemming from the same initial ν_τ .

The decay of the RHN also constitutes a new avenue for detection. Analogously with the τ , atmospheric decay via hadronic channels is likely to instigate an extensive air shower (EAS) that may be observed by detectors such as POEMMA and GRAND. Hence, in simulating the propagation described in this Section and computing effective areas and results for detectors, we must consider both the usual τ and the potential observable decay of the RHN.

4.1.2 Adapting TauRunner

To quantify the effects of our RHN model on Earth-traversing UHE τ neutrinos, we adapted the Python-based `TauRunner` program to simulate the processes described.

We introduced the right-handed neutrino N to `TauRunner`’s existing inventory of particle species and implemented its interactions with Standard Model particles accordingly, including the new mixing NC and CC interactions and the decay of the RHN.

Fig. 4.2 illustrates the possibilities open to a particle simulated by our adapted `TauRunner` program as it traverses a chord length through the Earth. The path choice at any given juncture is determined by Monte Carlo methods involving the

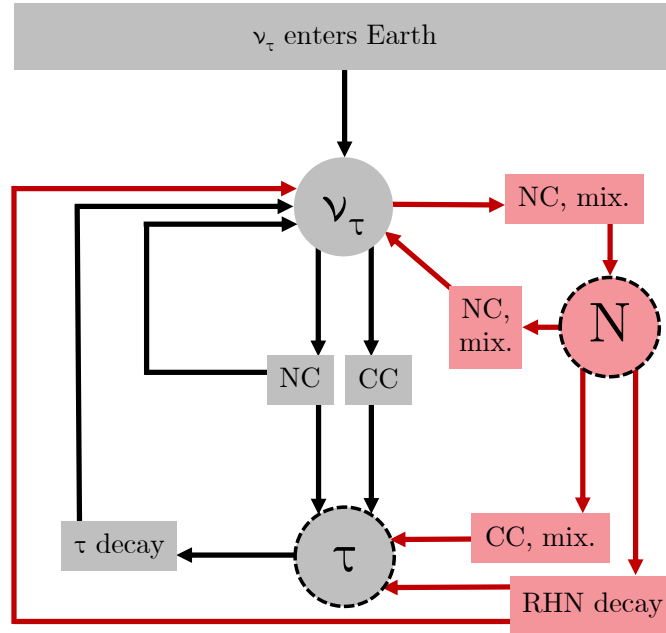


Figure 4.2: A flowchart illustrating the interactions and decays available to a particle in our simulations. Grey items are featured in the base version of `TauRunner`, while red items represent the BSM modifications implemented in our adapted version. Dashed bordering is applied to those particles that, having exited the Earth, may enable detection via an EAS in the atmosphere.

random sampling of distributions derived from the relevant cross sections, decay widths, and branching ratios.

For a given set of model parameters (the RHN mass m_N and the mixing angle θ_{mix}) and simulation specifications as before (the number n and energy E_ν of the initial sample of UHE τ neutrinos, and the emergence angle θ_{em} determining the chord length they traverse through the Earth), our adapted `TauRunner` program provides as an output a list of all Earth-exiting particles and their energies.

4.1.3 Quantities of Interest

For both detectable species (the τ and the RHN), we calculate the number of exiting particles as a fraction of the number n of neutrinos in the initial ν_τ sample, henceforth known as P_{exit}^i for $i = \tau, N$. It should be noted that, while P_{exit} can be intuitively

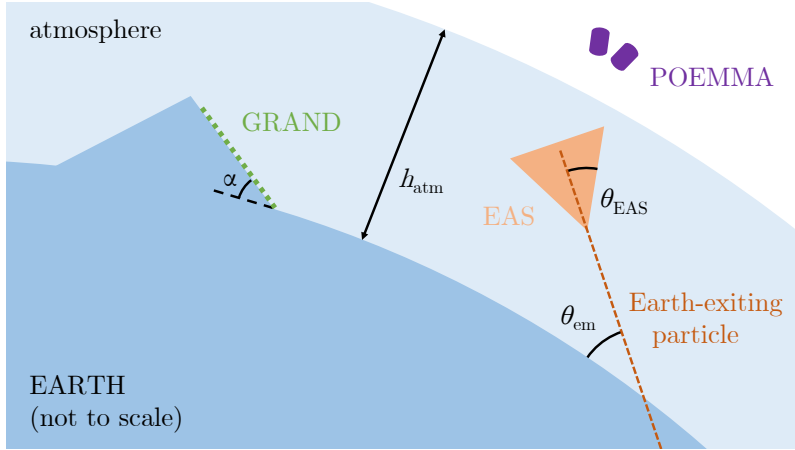


Figure 4.3: A schematic to illustrate the relevant geometry: the emergence angle θ_{em} , the EAS angle θ_{EAS} , and the atmospheric altitude h_{atm} . GRAND (with its incline of α) and the POEMMA satellites are additionally depicted.

regarded as the probability of an event resulting in an exiting particle of the given species, it does not correspond directly to a probability; one could, in principle, find that $P_{\text{exit}} > 1$ due to the production of multiple daughter particles by RHN decays. With the parameter ranges investigated, however, we generally expect $P_{\text{exit}} \ll 1$.

By running simulations over a range of values of the emergence angle θ_{em} , we sample a function $P_{\text{exit}}(\theta_{\text{em}}|E_\nu)$, where E_ν is the initial ν_τ energy for a given simulation. Here, the emergence angle θ_{em} is defined as the angle between the particle's track and the plane tangential to the Earth's surface at the point of the particle's exit, as illustrated in in Fig. 4.3. Low emergence angles describe particle tracks that shallowly skim the Earth, with the extreme of $\theta_{\text{em}} = 0^\circ$ representing a tangent to the Earth's surface, while high emergence angles describe particle tracks traversing deep chord lengths through the Earth's interior, with the extreme of $\theta_{\text{em}} = 90^\circ$ representing the full diameter.

When a UHE neutrino traverses a large distance through the matter of the planet's interior, it loses energy via numerous interactions, and in some cases can no longer be considered to have ultra-high energy. We define a successful 'exit' (in the calculation of P_{exit} , for example) as the particle exiting with energy above a certain threshold set several orders of magnitude below the initial energy E_ν . Our adapted version of

the `TauRunner` program implements this with a chosen minimum-energy threshold; any particle whose energy falls below this threshold is neglected by the simulation.

For the definition of P_{exit} used henceforth, this cut-off is set 2.5 orders of magnitude below the energy E_ν of the initial ν_τ sample. Where $E_\nu = 10$ EeV, for example, P_{exit} is defined to include only those particles that exit with energy $E_{\text{exit}} \gtrsim 32$ PeV.

Those particles that did survive with sufficient energy were counted into bins according to their exit energy E_{exit} , as the distribution of exit energies was useful for detector simulations later.

4.2 Results

The following sections present and discuss the results of our Earth-traversing UHE ν_τ simulations.

4.2.1 Simulation Results

The adapted `TauRunner` was run for a range of geometries between $\theta_{\text{em}} = 0.1^\circ$ and $\theta_{\text{em}} = 90^\circ$, with various choices for the model parameters m_N and θ_{mix} and for various values of the initial energy E_ν .

Fig. 4.4 shows the variation of P_{exit} with θ_{em} for different choices of the mixing angle and initial ν_τ energy E_ν , for a chosen RHN mass of $m_N = 3$ GeV. Solid lines depict the $P_{\text{exit}}(\theta_{\text{em}}|E_\nu)$ calculated for RHNs, P_{exit}^N , and dashed lines depict that for charged τ leptons, P_{exit}^τ .

4.2.2 Discussion of Small Emergence Angles

At small emergence angles θ_{em} , corresponding to particle tracks that shallowly skim the Earth, the mixture of detectable particles is vastly dominated by the charged τ leptons expected in the Standard Model case. The comparatively minuscule quantity

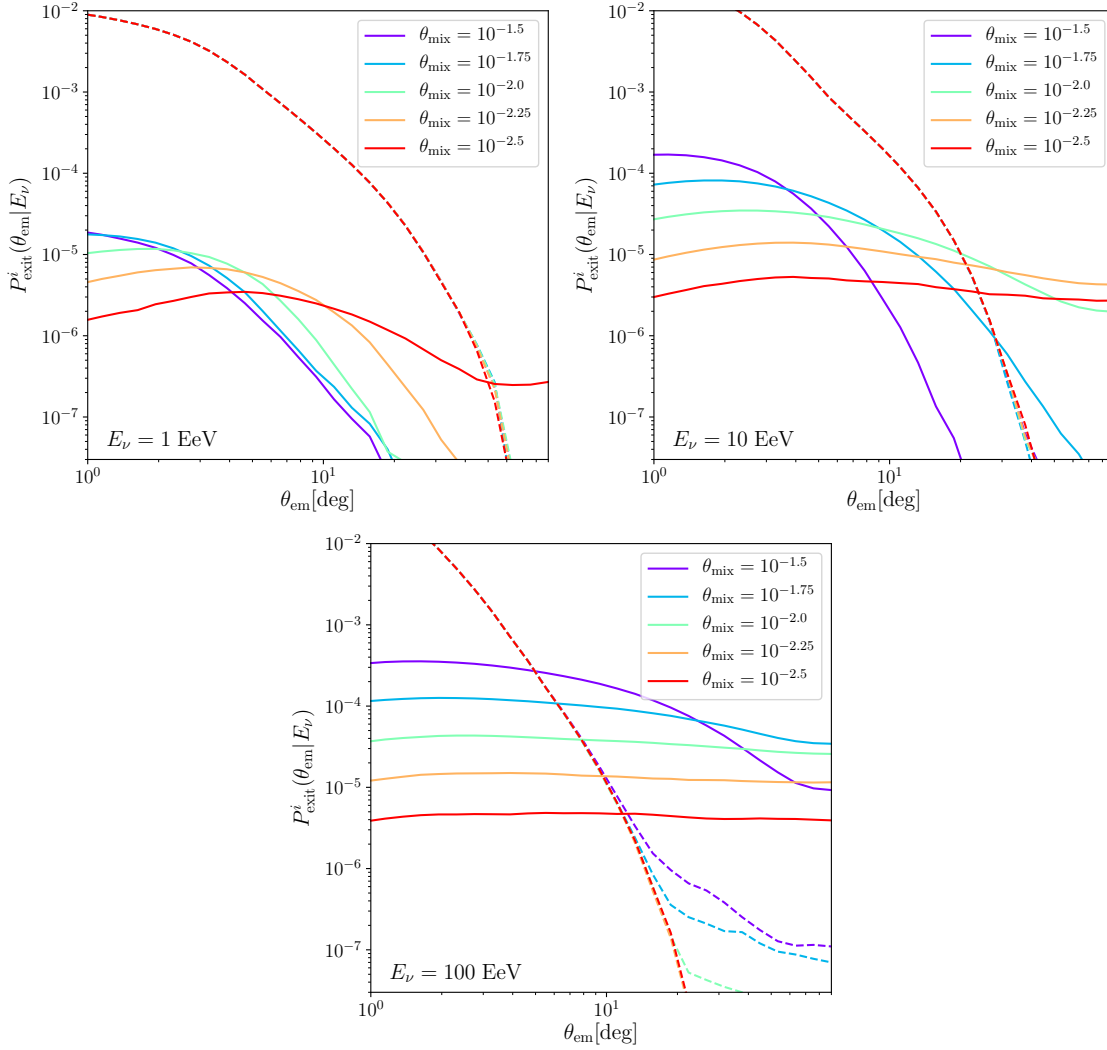


Figure 4.4: The results of our Earth-traversing UHE neutrino simulations, showing the variation of P_{exit}^i with the emergence angle θ_{em} , for a chosen RHN mass of $m_N = 3$ GeV and various choices of the mixing angle θ_{mix} , simulated for different initial neutrino energies E_ν in the respective plots. Solid lines are for RHNs ($i = N$) and dashed lines are for charged τ leptons ($i = \tau$).

of RHNs increases with θ_{mix} , as a higher value of the mixing parameter results in more mixing NC interactions capable of producing RHNs.

For the short paths through the Earth’s interior constituted by tracks of small emergence angles, this RHN production is the dominant process influencing P_{exit}^N . RHN decay is less significant at these angles, as any RHNs produced travel such short distances before exiting the Earth that decay over such scales is relatively unlikely.

As a result, higher values of θ_{mix} (colours closer to the violet end of the spectrum in Fig. 4.4) produce a larger P_{exit}^N .

4.2.3 Discussion of Large Emergence Angles

At larger emergence angles θ_{em} , corresponding to longer chords, the Earth becomes effectively opaque to UHE neutrinos in the Standard Model scenario.

While the SM τ flux (i.e. P_{exit}^τ for low θ_{mix} , depicted by colours closer to the red end of the spectrum in Fig. 4.4) drops away at these large distances through the Earth, higher choices of the BSM parameter θ_{mix} (colours closer to the violet end of the spectrum in the figure) allow for a small flux to be retained, especially at higher energy E_ν . The influence of the BSM physics—namely regeneration via the production, propagation, and decay of RHNs—permits the survival of more particles that may exit as τ leptons. As demonstrated in the third plot of Fig. 4.4, greater values of θ_{mix} (depicted by colours closer to the violet end of the spectrum) improve this τ lepton ‘tail’.

The right-handed neutrino flux (solid lines, depicting P_{exit}^N) starts to dominate over this τ tail (dashed lines, depicting P_{exit}^τ) at higher energies E_ν , as can be seen in the third plot of the figure. Neutrinos of the highest energies, traversing the deepest chords of the Earth, are therefore more likely to exit as RHNs than as τ leptons.

While for Earth-skimming events (small θ_{em}), the RHN flux was improved by increasing the mixing parameter θ_{mix} , at longer chord lengths (large θ_{em}) a higher

mixing parameter begins to instead deplete it. This is because, over these length scales, the decay of the RHN while still traversing the Earth becomes significant, rivalling the production of the RHN (via mixing NC interactions) in its effect. On the one hand, a higher mixing parameter allows for increased production of RHNs, but on the other hand, it then depletes the resulting flux of RHNs via decay, by reducing the average length λ_N over which the RHN may propagate before decaying (as previously plotted in Fig. 2.3). In many cases, for long chord lengths, this latter effect dominates. We see in the first plot of Fig. 4.4, for example, that the ordering of the coloured lines becomes entirely inverted as we probe larger emergence angles. Thus, where higher values of θ_{mix} (colours closer to the violet end of the spectrum in Fig. 4.4) previously resulted in a larger P_{exit}^N due to increased production, they now inhibit P_{exit}^N due to increased decay.

The significance of the RHN flux and BSM τ flux relative to the SM τ background at higher emergence angles renders this region of θ_{em} an area of particular interest. In later parts of this work, we especially focus on these deeper particle track geometries.

Chapter 5

Detector Simulations and their Results

Having simulated the effects of our RHN model on Earth-traversing UHE neutrinos, we must investigate the its influence on detection results.

5.1 Detection Methodology and Effective Area

Our general strategy is to simulate the detection of the fluxes obtained in Chapter 4 at large-volume observatories. In particular, we choose detectors that observe the extensive air showers (EASs) produced by the decaying particles in the atmosphere, as described in Section 3.3.1. This category includes balloon experiments such as ANITA or PUEO, space-based observatories like POEMMA, and ground-based detectors like GRAND, Trinity, or TAROGE-M, as summarised in Table 3.1.

Within this detection framework, a particle (τ or N) exiting the Earth must meet two conditions to yield a detectable signal. Firstly, it must decay within the atmosphere to produce a developed EAS; decays beyond a certain atmospheric length scale will not be detected. Secondly, the detector (or part of it, as is the case with the radio antennae of GRAND) must fall within the cone of the EAS and its electromagnetic signal.

Following the prescription of Ref. [31], the effective area we calculate for a given detector and a given particle of choice $i = \tau, N$ may be summarised as

$$\frac{d^3 \mathcal{A}_{\text{eff}}^i}{d\Omega_\nu dE_\nu} = \int R_E^2 (\vec{n}_E \cdot \vec{n}_\nu) d\Omega_E \int dE_{\text{exit}} \frac{dP_{\text{exit}}^i(\theta_{\text{em}}|E_\nu)}{dE_{\text{exit}}} \int d\ell_{\text{dec}} \frac{dP_{\text{dec}}^i(\ell_{\text{dec}}|E_{\text{exit}})}{d\ell_{\text{dec}}} P_{\text{det}}^i(\vec{r}_{\text{dec}}, E_{\text{exit}}) \quad (5.1.1)$$

where R_E is the radius of the Earth, and the integrals applied reflect a range of geometries for consideration.

The differential solid angle $d\Omega_\nu$ reflects the orientation of the incoming flux, with direction (θ_ν, ϕ_ν) represented by the normal vector \vec{n}_ν . The dependence on $d\Omega_\nu$ thus represents a variation over the celestial sphere as we consider various possible orientations of neutrino flux.

The differential solid angle $d\Omega_E$ reflects the geometry of the Earth, with a point of colatitude and longitude (θ_E, ϕ_E) represented by the normal vector \vec{n}_E . The integration over Ω_E thus represents a scan over the Earth's sphere to consider all possible points at which a neutrino might be incident.

The emergence angle θ_{em} , used in our simulations and present in Eq. (5.1.1) as an argument of the differential form of P_{exit} , is an implicit function of the angles $(\theta_\nu, \phi_\nu, \theta_E, \phi_E)$. The differential form of $P_{\text{exit}}^i(\theta_{\text{em}}|E_\nu)$ represents the results of our simulations of Earth-traversing UHE neutrinos, to be integrated over the described range of exit energy E_{exit} .

After a particle $i = \tau, N$ has exited the Earth with energy E_{exit} , its probability of decay after travelling some distance ℓ_{dec} can be expressed as

$$\frac{dP_{\text{dec}}^i(\ell_{\text{dec}}|E_{\text{exit}})}{d\ell_{\text{dec}}} = \frac{1}{\lambda_i(E_{\text{exit}})} \exp\left(-\frac{\ell_{\text{dec}}}{\lambda_i(E_{\text{exit}})}\right) \quad (5.1.2)$$

where $\lambda_i(E_{\text{exit}})$ is the decay length of that particle species. Given a decay at a location \vec{r}_{dec} determined by ℓ_{dec} and the geometry $(\theta_\nu, \phi_\nu, \theta_E, \phi_E)$, we can define the

probability that it triggers a detection, $P_{\text{det}}^i(\vec{r}_{\text{dec}}, E_{\text{exit}}|\theta_\nu, \phi_\nu, \theta_E, \phi_E)$, to be calculated from simulations of the detector geometry.

The integration over ℓ_{dec} thus represents a scan along the path of an Earth-exiting particle, integrating over (actual) decay length, with regard to the probability of triggering detection given a decay at any particular point.

5.2 GRAND Simulations

We first perform this procedure for the case of GRAND, the aforementioned ground-based observatory comprising an array of radio antennae spread over mountainous slopes.

5.2.1 Implementation

In order to model the physical arrangement of GRAND, we consider a plane inclined at an angle α to the ground at the detector site. We establish a semicircular region of radius R_{det} within this plane, positioned such that the straight edge constituted by the semicircle's diameter is in contact with the ground along the base of the slope. This configuration thus represents a region of detectors over an inclined area of $\pi R_{\text{det}}^2/2$. We choose the radius of the semicircular region to have radius $R_{\text{det}} = 80$ km in approximate accordance with GRAND's expected detector area of 10,000 km² per site, and choose an inclination of $\alpha = 3^\circ$ to describe a realistic slope available for GRAND's use.

For a given initial energy E_ν , our simulation of GRAND uses the results of our adapted **TauRunner** program to determine $dP_{\text{exit}}^i/dE_{\text{exit}}$ for each particle species $i = \tau, N$, interpolated over the full range of the elevation angle θ_{em} . We then follow the prescription described in Section 5.1; for each exit energy bin, corresponding to an average decay length of the exiting particle, the probability of decay is calculated at successive points along the particle's path through the atmosphere after exiting

the Earth, and, at each point, it is determined whether or not such a decay would trigger a detection in any part of the detector region via the radiative cone produced by its EAS. Keeping only those points where a decay would trigger a detection, the decay probabilities are summed in order to integrate along the particle's path (corresponding to the integration over ℓ in Eq. (5.1.1)), and the results for the respective energy bins are combined (corresponding to the integration over E_{exit}) to calculate an overall probability of detection for any given set of angles describing the particle's trajectory.

The simulation then iterates over varying incoming particle orientations (corresponding to a grid over the celestial sphere) and over a grid of impact locations on the Earth's surface, thus integrating over geometric configurations to calculate a total effective area for the detector for a given initial neutrino energy E_ν . The resulting effective area is multiplied by a factor of 20 to account for the multiple detectors intended for construction by the GRAND collaboration.

5.2.2 Results and Discussion

Fig. 5.1 shows the results we obtained for the GRAND effective area, simulated for varying mixing angle θ_{mix} , integrated over the incoming direction Ω_ν , and for different choices of the initial neutrino energy E_ν .

As can be seen in the figure, the effective area for detecting charged τ leptons, $\mathcal{A}_{\text{eff}}^\tau$, is mostly insensitive to the value of θ_{mix} , as any BSM effects are dominated by the SM τ flux. The predicted effective area for detecting RHNs, $\mathcal{A}_{\text{eff}}^N$, increases with θ_{mix} , but is many orders of magnitude smaller than that for τ leptons, and hence cannot produce a significant signal relative to the SM background.

This outcome results mainly from geometric constraints. The range of emergence angles θ_{em} accessible to GRAND is narrow, limited by the shallow inclination of the detector. In the configuration we simulated, for example, it is clear that GRAND cannot observe particles exiting the Earth with $\theta_{\text{em}} \gtrsim \alpha$, with the only margin of error

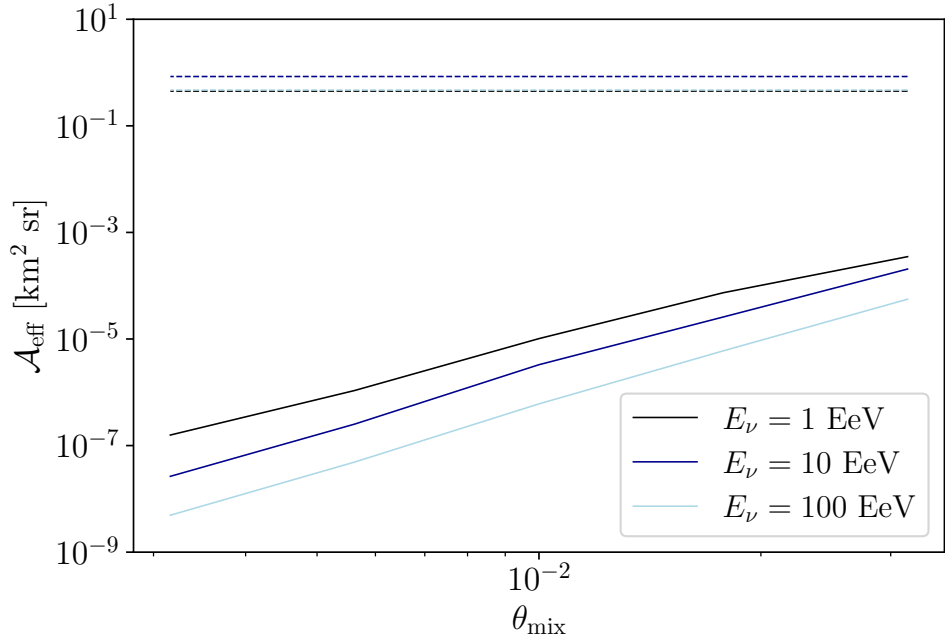


Figure 5.1: The variation of the effective area $\mathcal{A}_{\text{eff}}^i$ calculated from our GRAND simulations with the mixing angle θ_{mix} , for charged τ leptons ($i = \tau$, dashed) and RHNs ($i = N$, solid), for different choices of the initial neutrino energy E_ν .

It should be noted for clarity that the dashed black line and dashed light blue line for $E_\nu = 1 \text{ EeV}$ and $E_\nu = 100 \text{ EeV}$ τ leptons respectively are overlapping.

arising from the opening angle θ_{EAS} of the extensive air shower and radiative cone. Thus, for any realistic value of α , the inclination of the mountainous slope, detection is constrained to small emergence angles at which the SM τ flux is dominant, as we established in Chapter 4 and as is clear in Fig. 4.4. At these Earth-skimming angles, corresponding to very short and shallow tracks, UHE neutrinos have a good chance of exiting the Earth after few interactions with nucleons, allowing for a strong τ flux but rendering RHNs difficult to produce given the statistics available.

For an isotropic GZK spectrum of UHE neutrinos, we found, using current limits from Auger, that even a detector with inclination $\alpha = 30^\circ$, which is far beyond realistic values implementable on Earth with a detector array area comparable to that of GRAND, a detector analogous to GRAND would only detect $\mathcal{O}(1)$ BSM events over a five-year observation period, integrated over all emergence angles and exit energies.

An alternative scenario could involve GRAND observing a transient source bright enough that its UHE neutrino flux is significantly higher than the aforementioned GZK flux. In this case, however, the neutrino source would be localised to one direction of origin in the sky; given the narrow range of emergence angles discussed, a GRAND-like detector would need to be quite precisely aligned with the source to provide results. In the context of the 20 individual detectors discussed in the planning of GRAND200k, it is certainly possible that at least one could be situated such that the source would fall within its Earth-skimming window, but, on the other hand, observation by only one array out of all those available would suppress the effective area by a factor of 20. In light of both the improbability of bright enough a source and the penalty incurred by using only one or few of the individual detectors to observe a localised transient, we rule out this scenario.

In summary, it appears that a GRAND-like observatory would likely not provide useful results or constraints for the particular BSM model considered in this thesis, in the context of Earth-traversing UHE neutrinos, as will be discussed in comparison with our results for POEMMA in Section 5.4.

5.3 POEMMA Simulations

We now apply a similar procedure to POEMMA, the aforementioned satellite-based observatory.

5.3.1 Implementation

Given its very high altitude, POEMMA has a large field of view over which to observe the Cherenkov light produced by extensive air showers in the atmosphere. Depending on the mode used, it can probe very small and very large emergence angles θ_{em} , and, at such great distances above the production of an EAS, the resulting Cherenkov cone may spread over vast areas, enhancing the effective area for detection in spite of the detector's relatively small spatial extension compared to a larger array like that of GRAND.

A comprehensive analysis for computing the probability of detection, P_{det}^i for $i = \tau, N$, would entail precisely simulating the development of an extensive air shower in the atmosphere and estimating the resulting photon flux in order to run a thorough detector simulation. Such an analysis would require the detector simulation programs developed by the POEMMA collaboration to reach robust predictions, and so is beyond the scope of this work.

Instead, we made simplified but realistic approximations to carry out a more feasible analysis, hopefully motivating a more thorough analysis with the proper detector simulations in future. Any particle decay was considered to trigger a detection, excepting those that met certain exclusion criteria: the particle exited with energy $E_{\text{exit}} < 0.1$ EeV (these were found not to significantly contribute to our results, and so were deemed computationally wasteful); the detector did not fall within the Cherenkov cone of the EAS; or the particle decayed beyond the lower atmosphere where an EAS would develop sufficiently, as defined by a maximum altitude h_{atm} .

In truth, the capacity of a given decay to produce an EAS varies continuously with the decay altitude, as does the opening angle of the resulting Cherenkov cone.

Additionally, the photon signal produced can be attenuated by a thick layer of atmosphere between the EAS and POEMMA. Refs. [29, 82, 83] provide a more detailed and extensive exploration of the variables involved and the ability of air- or satellite-borne observatories, including POEMMA, to detect a given EAS.

Using figures stated in these sources for guidance, we chose to assume a fixed value for the opening angle, θ_{EAS} , carrying out our simulations for a set of values in the range

$$1.5^\circ \leq \theta_{\text{EAS}} \leq 3.5^\circ \quad (5.3.1)$$

to account for and analyse any error incurred by this fixing. Similarly, we chose to assume a fixed value for the maximum altitude at which an EAS can be produced, once again using a spread of values, choosing for this parameter the range

$$15 \text{ km} \leq h_{\text{atm}} \leq 25 \text{ km}. \quad (5.3.2)$$

For clarity, these two parameters were included in the schematic illustration of Fig. 4.3 in the previous chapter.

With these approximations in place, the integration procedure utilised throughout this chapter was applied to geometric simulations of POEMMA to obtain an effective area.

5.3.2 Results and Discussion

Fig. 5.2 illustrates the POEMMA results with a plot of the effective area (averaged over energies in the range 1–100 EeV) against the mixing angle parameter, for a chosen geometry of $\theta_{\text{em}} = 70^\circ$, shown for various choices of the RHN mass.

As we increase the mixing angle θ_{mix} —that is, bolster the presence of the BSM physics—the effective area tends to steadily increase (fairly uniformly with respect

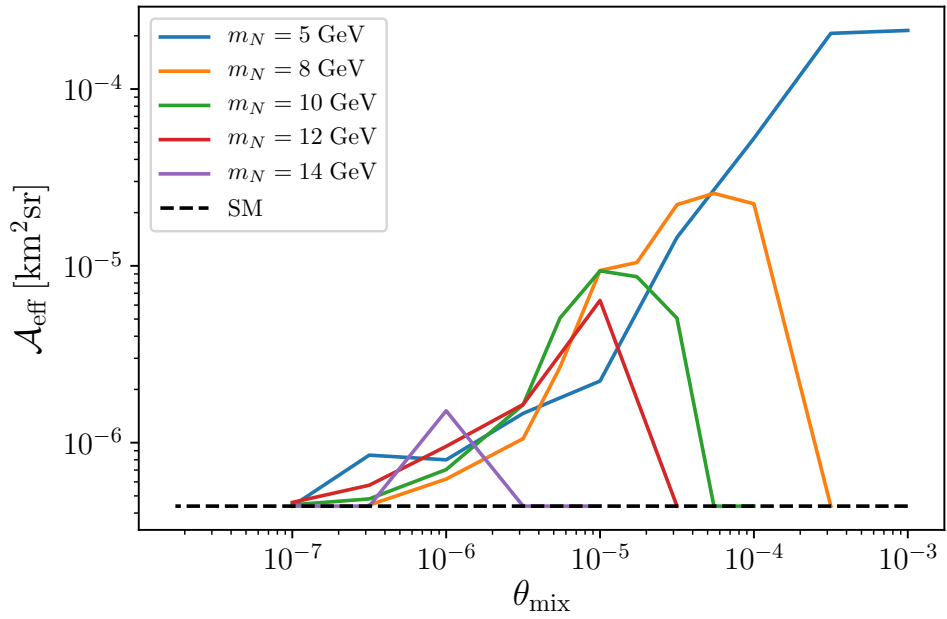


Figure 5.2: The total effective area of POEMMA in our scenario (averaged over energy bins in the range 1–100 EeV) against the mixing angle parameter θ_{mix} , for a chosen geometry of $\theta_{\text{em}} = 70^\circ$, shown for various choices of the RHN mass m_N

to the mass), reach a peak, and rapidly fall to the SM value. Heavier masses shift this peak further to the left (and thus also reduce its height); for the lightest mass shown, $m_N = 5$ GeV, the effective area increases monotonically with the mixing angle in the domain shown, but for the heavier masses, the lines of Fig. 5.2 peak earlier and earlier until the heaviest mass of $m_N = 14$ GeV shows only a small peak above the SM, situated at a low mixing angle.

This is congruent with expectations. A very low mixing angle inhibits the production of RHNs in the first place, and so the BSM physics can have little influence; additionally, those RHNs that might be produced have such a long decay length (see Fig. 2.3 for the effect of mixing angle on decay length) that they are unlikely to decay in the appropriate altitude range of the atmosphere to produce an EAS and trigger a detection.

Increasing the mixing angle produces more RHNs, and improves the probability of decay and hence detection; this is reflected in the initial increase seen in Fig. 5.2.

As the mixing angle becomes too high, however, RHNs decay so readily that they are largely unable to exit the Earth; this is reflected in the drop after the peak.

Heavier masses are associated with shorter-lived RHNs, and so increasing m_N bolsters this latter effect, and for the heavier masses we see it coming into play earlier with respect to θ_{mix} , reflected in the shifting of the peak.

5.4 Detector Comparisons

5.4.1 Key Differences

GRAND and POEMMA—or, more broadly, GRAND-like detectors and POEMMA-like detectors—are qualitatively and quantitatively different. The former is ground-based and has a large spatial extent (a detector array with an area of $\sim \mathcal{O}(10^5)$ km²), but is located at a low altitude ($\sim \mathcal{O}(1)$ km), while the latter, as a satellite-based detector, has a much smaller spatial extent ($\sim \mathcal{O}(1)$ m²) but is located at a much higher altitude ($\gtrsim \mathcal{O}(100)$ km).

A major consequence of these differences is the detectors' respective fields of view. GRAND observes a narrow range of small emergence angles close to the horizon, making it ideal for measuring and studying the (Standard Model) τ flux produced by Earth-skimming UHE neutrinos. POEMMA, on the other hand, is capable of probing large emergence angles corresponding to deeper chords of the Earth, where the strongest influence of our BSM model comes into play, as was concluded at the end of Chapter 4.

Additionally, the altitudinal contrast between the two also alters the distances over which a particle can travel before decaying while still subsequently triggering a detection. To produce an EAS observable by POEMMA, a detectable particle may decay anywhere in the lower atmosphere (implemented by the maximum altitude h_{atm} in our approximations), and the long section of a particle's path between exiting

the Earth and leaving this region provides ample opportunity for decay and thence detection.

In the case of GRAND, on the other hand, the relevant section of a given particle track is generally much smaller. Unless a particle skims the Earth with such a slight emergence angle that it can travel near-parallel to the ground over a longer distance, it must exit the Earth relatively close to the detector in order to have a chance of decaying such that the radiative cone is oriented appropriately, and this greatly reduces the distance over which a decay is viable for detection.

As the RHN decay length is highly sensitive to the model parameters (the RHN mass m_N and the mixing angle θ_{mix}), permitting only a narrow window for decay on a particle's journey greatly inhibits the detectability of the RHN in particular for vast regions of the parameter space. It is somewhat paradoxical to hope for a significant signal of RHNs produced in the Earth that, on the one hand, manage to exit the Earth before decaying, but then, on the other hand, are subsequently likely to decay within a short distance of their emergence for detection. Values of the model parameters that render the RHN short-lived will result in RHNs decaying in the Earth shortly after production, inhibiting the flux exiting the Earth; those that render the RHN long-lived will result in RHNs travelling too far after exiting the Earth before decaying to trigger a detection at a closely-situated detector. A distantly-situated detector like POEMMA improves the distance ratio between these two parts of a particle's journey, and gives detectable particles an opportunity to decay at some point over the much larger atmospheric distance.

5.4.2 Outcome

From the results presented, we find that POEMMA is capable of producing a relevant signal in the context of the BSM model discussed (Fig. 5.2 depicts significant deviations from the SM prediction), while GRAND is not (Fig. 5.1 illustrates that GRAND's results showed no significant deviation in the detection of charged τ

leptons, and poor, subdominant statistics for the RHNs).

This is primarily due to the ranges of θ_{em} probed. At the Earth-skimming emergence angles observed by GRAND, UHE neutrinos can readily survive their journeys with little energy loss, producing a dominant τ flux relative to which the influence of the BSM physics is negligible. At the depths probed by POEMMA—at $\theta_{\text{em}} = 70^\circ$, for example, as used for the results of Fig. 5.2—the Earth is effectively opaque in the context of the Standard Model, and so the results of adding BSM physics to the system of Earth-traversing UHE neutrinos can produce a good signal.

It should be emphasised that the issues and comparisons discussed here are posed specifically in light of our particular BSM model. GRAND, like the other detectors listed, shows great promise in the wider study of UHE neutrinos, and could also be competitive in the search for other BSM scenarios. Models involving an extended spectrum of heavy particles with decay length $\lambda \lesssim \mathcal{O}(1\text{--}10)$ km, such as string theory or models involving extra dimensions (see e.g. Refs. [84–87]), could provide contexts where BSM particles can both readily exit the Earth and have a good chance of decaying within a short distance and thus triggering a detection at a GRAND-like detector. Future work could involve studies of how such models would influence results at large-volume detectors of UHE neutrinos, such as GRAND, POEMMA, and the others listed in Table 3.1, but in this work we focus on the RHN model established.

Chapter 6

Final Results and Discussions

We have established that the RHN model discussed can indeed affect the capacity of UHE neutrinos to successfully exit the Earth, and influence the distributions measured at large-volume detectors such as, in particular, POEMMA. We must now determine which scenarios—what values of the model parameters, and which UHE neutrino sources in the cosmos—will result in significant deviations from the Standard Model results.

6.1 Methodology for Probing Parameter Space

The numbers and measurements possible depend on the flux and direction of the incoming neutrinos. As discussed, observations at small emergence angles, $\theta_{\text{em}} \lesssim \mathcal{O}(10)^\circ$ will be dominated by the UHE τ flux expected in the SM case, unaffected by the BSM physics. While this is not directly helpful for probing BSM phenomenology, it is incredibly useful for studying the SM situation: determining the flux and acquiring information about the neutrino source.

Given the multiplicity of detectors around the globe searching for UHE neutrinos at small emergence angles, several detectors could simultaneously observe and measure the flux, whether from a given transient or from a diffuse cosmogenic background. Even POEMMA itself comprises two separate satellites that, depending on timing

and geometry, could potentially observe a source at different respective emergence angles.

We thus assume henceforth that, regardless of the nature of the source, the flux of incoming neutrinos considered is known, having been determined by measurements at small emergence angles. We must then investigate whether POEMMA can observe such a source at a large emergence angle with suitable statistics, and explore the regions in the space of model parameters m_N and θ_{mix} where the impact of the BSM physics is significant.

6.1.1 Utility of Diffuse and Transient Sources

As was introduced in Section 3.1, UHE neutrinos received at the Earth may originate from a constant and isotropic flux, such as that expected for cosmogenic GZK neutrinos, or from transient events, localised in space with finite durations.

A diffuse flux has been constrained by ANITA [65], IceCube [66], and Auger [67]. Given its expected sensitivity, even with a full field of view, POEMMA is forecast to detect $\mathcal{O}(10\text{--}100)$ events over a five-year observation period [22], and these will be detected preferentially at small emergence angles. This scenario provides insufficient statistics for the BSM model's influence to become apparent, and so we rule out a diffuse flux as an avenue for study here. Instead, we turn to transient events.

As mentioned, POEMMA is capable of performing efficient target-of-opportunity (ToO) observations [81] to view transients. It is expected to detect over a hundred events when observing a burst of UHE neutrinos at $\mathcal{O}(10)$ Mpc, and, given that the flux from a localised source scales with the inverse square of the distance, an astrophysical event closer to the Earth's neighbourhood would increase this number by several orders of magnitude.

It can be seen in Fig. 4.4 that an incoming neutrino of energy $E_\nu = 100$ EeV can produce an Earth-exiting RHN at a large emergence angle θ_{em} with a probability of $\mathcal{O}(10^{-4})$. A transient burst close enough (~ 1 Mpc from Earth) that POEMMA

would detect $\mathcal{O}(10^4)$ events would therefore potentially result in $\mathcal{O}(1)$ BSM events at a large emergence angle $\theta_{\text{em}} \gtrsim 10^\circ$.

6.1.2 Choice of UHE Neutrino Source

A gamma ray burst (GRB) is a high-energy explosion usually precipitated by the collapse of a massive star or a merger of compact objects. GRBs provide exciting targets for multi-messenger astronomy; the associated events have been detected via gravitational waves [88] and are expected to provide sources of UHE cosmic rays and neutrinos [89, 90].

In October 2022, the Gamma-ray Burst Monitor (GBM) [91], the Burst Alert Telescope (BAT) [92], the Fermi Large Area Telescope (LAT) [93] and the LHAASO collaboration [94] detected an extraordinarily bright GRB located 637 Mpc from Earth, now designated GRB 221009A [95]. Various studies [4, 96] developed models to explain the measurements and observations made, including the timing and energy distribution of the gamma rays and the absence of any muon neutrino tracks associated with the event at IceCube [97]. In light of these models, it is predicted that the event would have produced UHE neutrinos of energies up to $\mathcal{O}(100)$ EeV.

We henceforth take GRB 221009A as a benchmark example, and use the UHE neutrino fluence derived in Ref. [4] in our analysis. The flux can be rescaled by a factor $(D_{\text{GRB221009A}}/D)^2$, where $D_{\text{GRB221009A}}$ is the distance from Earth at which the GRB 221009A event occurred, in order to obtain the appropriate flux for a similar event at a distance D . Fig. 6.1 depicts the expected energy fluence $E_\nu \mathcal{F}_\nu$ as a function of the neutrino energy E_ν , as expected from a 221009A-like event at various distances.

In our analysis, we consider distances ranging roughly from the size of the Milky Way (~ 30 kpc) to the distance to the Andromeda Galaxy (~ 770 kpc). Other detectors would likely observe these nearby events, subject to geography (see e.g. Fig. 17 of Ref. [98] for a good overview of their respective sensitivities).

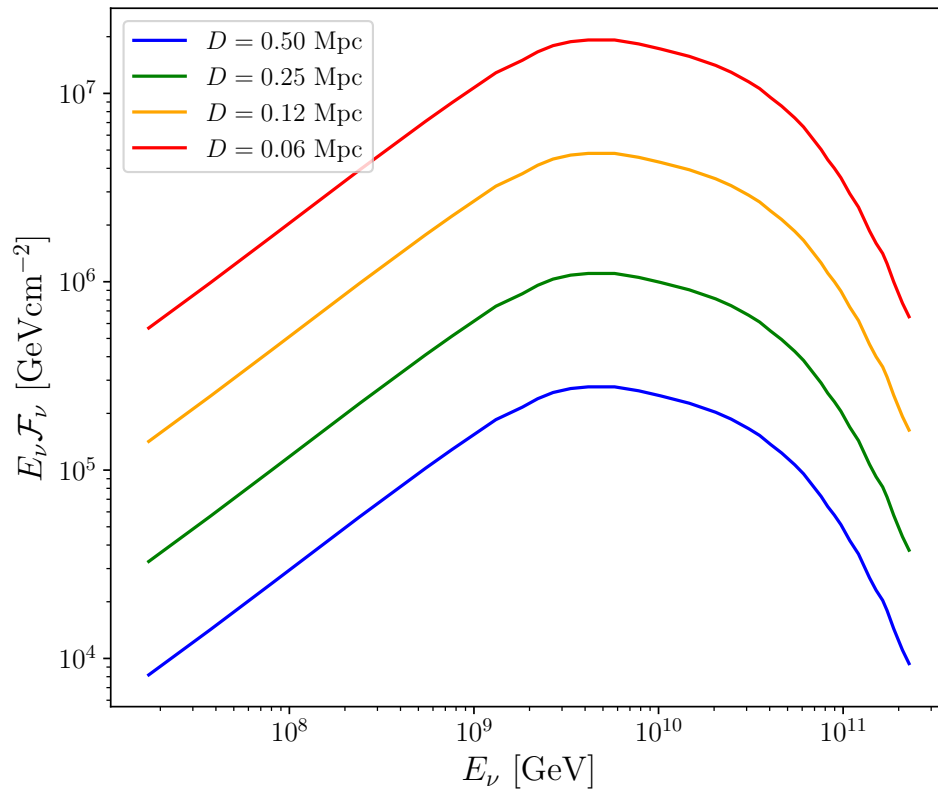


Figure 6.1: The neutrino fluence expected from a 221009A-like GRB, as sourced from Ref. [4], rescaled according to the distance D from Earth

GRBs at such proximity are expected to be relatively rare, but in the case that such an event might occur, the neutrino flux received on Earth could provide a compelling test of new physics.

6.1.3 Strategy and Statistical Approach

In summary, we consider POEMMA pointing at a transient event at some large emergence angle, corresponding to a large distance through the Earth for particles to traverse, while other large-volume detectors are able to evaluate the flux via observations at small emergence angles.

Using the `TauRunner` simulations, we tested that, at large emergence angles $\theta_{\text{em}} \gtrsim 60^\circ$, the SM background is zero, to a precision of $\mathcal{O}(10^{-10})$ in the exit probability for all E_{exit} bins considered. We hence took the SM exit probability to be 10^{-10} at these large emergence angles.

Using this and the UHE neutrino fluence above, we used our `TauRunner`-based Monte Carlo simulations for Earth-traversing UHE neutrinos and our detector simulations to probe the $(m_N, \theta_{\text{mix}})$ parameter space of our model, calculating numbers of events for both SM and BSM particles and demanding the criterion that the BSM signal deviate from the SM background by 3σ , corresponding to a confidence level of 99.7%.

6.2 Results

6.2.1 Key Results and Discussions

The plot in Fig. 6.2 shows the results of our parameter search in the case of an event at emergence angle $\theta_{\text{em}} = 60^\circ$, considering a 221009A-like transient source at various distances D , with the detection criteria restricted to include only particles that exit the Earth with energies in the range $10 \text{ EeV} \leq E_{\text{exit}} \leq 100 \text{ EeV}$ (first panel) and then in the slightly broader range $1 \text{ EeV} \leq E_{\text{exit}} \leq 100 \text{ EeV}$ (second panel). Each

line marks the extent of the region in which our statistical criteria were met, and thus demonstrates the region in which there was a significant BSM signal for each respective value of D .

Here we have borrowed the notation $U_{N\tau}$ for the mixing parameter from the relevant literature, corresponding to our mixing parameter $\sin\theta_{\text{mix}}$; thus $|U_{N\tau}|^2 \approx \theta_{\text{mix}}^2$.

It can be seen from the figure that different values of m_N and θ_{mix} can produce detectable signals in different ranges of E_{exit} . It is clear, for example, that for the larger RHN masses ($m_N \approx 12\text{--}14$ GeV), the search considering only the $10 \text{ EeV} \leq E_{\text{exit}} \leq 100 \text{ EeV}$ range can comfortably probe to relatively low mixing angles, with the widened E_{exit} range of the second panel producing a negligible additional contribution, while for the smaller RHN masses ($m_N \approx 2\text{--}5$ GeV), it is only when the E_{exit} range is broadened that lower mixing angles can be probed, as seen from the additional protuberance visible in the leftward regions of the second panel.

We additionally plot the current limits and sensitivities for comparison from CHARM [5, 6] (based on the absence of heavy neutrinos in the neutrino beam, setting upper limits on the mixing for a range of masses below our regime of study), DELPHI [7] (based on upper limits on the branching ratio of heavy neutrino production in Z decay), and SHiP [8] (based on calculations of the signal that would result from decaying heavy neutral leptons produced by the decays of charm and beauty mesons). The sensitivity region of this last features both a lower boundary and an upper boundary, the lower corresponding to parameter values at which the decay length of the produced particle becomes much larger than the detector size (and so too few decays occur within the decay volume) and the upper corresponding to parameter values at which the decay length becomes comparable to the distance between the target and the decay volume (and so too few particles reach the decay volume, as a large proportion decay beforehand) [8].

The regions probed by our strategy appear to be competitive and complementary with these existing constraints, as well as with future HL-LHC searches [99] and

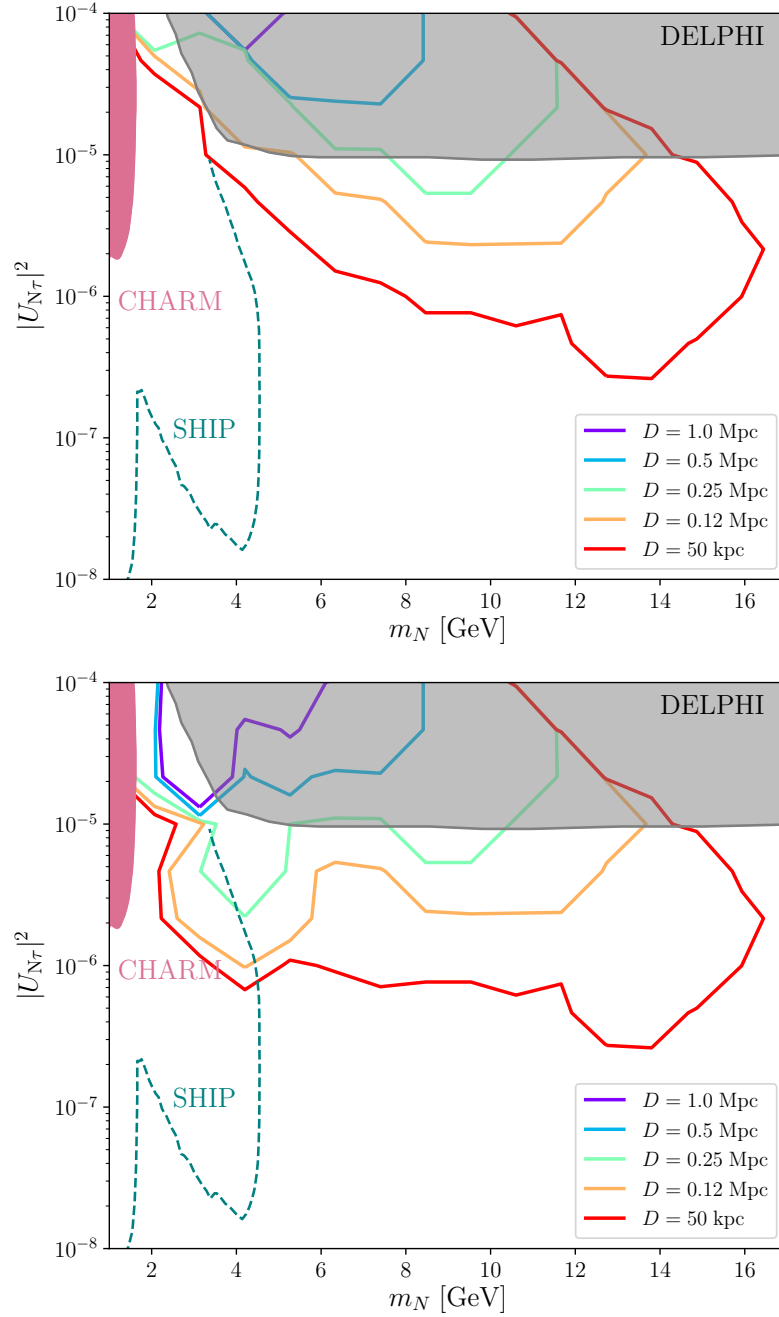


Figure 6.2: The sensitivity of the proposed RHN search using POEMMA, considering a transient event similar to GRB 221009A at an example emergence angle of $\theta_{\text{em}} = 60^\circ$, at various distances D .

The search is restricted to exit energies of $10 \text{ EeV} \leq E_{\text{exit}} \leq 100 \text{ EeV}$ for the results in the first panel, and to the broader range of $1 \text{ EeV} \leq E_{\text{exit}} \leq 100 \text{ EeV}$ for those in the second panel. The limits from CHARM [5, 6], DELPHI [7], and SHiP [8] are provided for comparison.

future dedicated UHECR searches for heavy neutral leptons that have been proposed [100].

An interesting feature of our results lies in the shape of the signal region in parameter space, providing not a hard upper bound in θ_{mix} , but probing a band in the $(m_N, \theta_{\text{mix}})$ -plane. This is reflective of the variation in effective area with θ_{mix} plotted in Fig. 5.2, and the two vying effects of θ_{mix} discussed accordingly in Section 5.3.2. These effects are comparable to those encountered in searches for BSM particles escaping supernovae (e.g. Ref. [101]); more generally, too strong a coupling with SM matter prevents the BSM particles from successfully exiting the body through which they propagate, while too weak a coupling inhibits both their production in the first place and their viability for observation.

6.2.2 Sensitivity to Approximations

As discussed in Section 5.3.1, we chose to approximate the effects of decay altitude on the capacity to develop a detectable EAS, and the continuous variation of the opening angle of the Cherenkov cone with altitude, by assuming a fixed maximum altitude h_{EAS} at which a decay can produce a detectable EAS, and a fixed opening angle θ_{EAS} , respectively.

For the sake of confidence in our results, it is of interest to review the impact of varying these parameters on the signals produced, in order to ensure that small variations in our approximations do not significantly alter our conclusions. Fig. 6.3 demonstrates the effects of changing these parameters in one example case among those we analysed, with the exit energies restricted to $10 \text{ EeV} \leq E_{\text{exit}} \leq 100 \text{ EeV}$, an emergence angle of $\theta_{\text{em}} = 60^\circ$ once again, and a chosen distance of $D = 50 \text{ kpc}$.

As is to be expected, a larger θ_{EAS} increases the sensitivity, as decaying particles will produce wider Cherenkov cones in which POEMMA is more likely to be located spatially. Similarly, a larger h_{atm} increases the sensitivity by increasing the distance over which a decay is viable for detection.

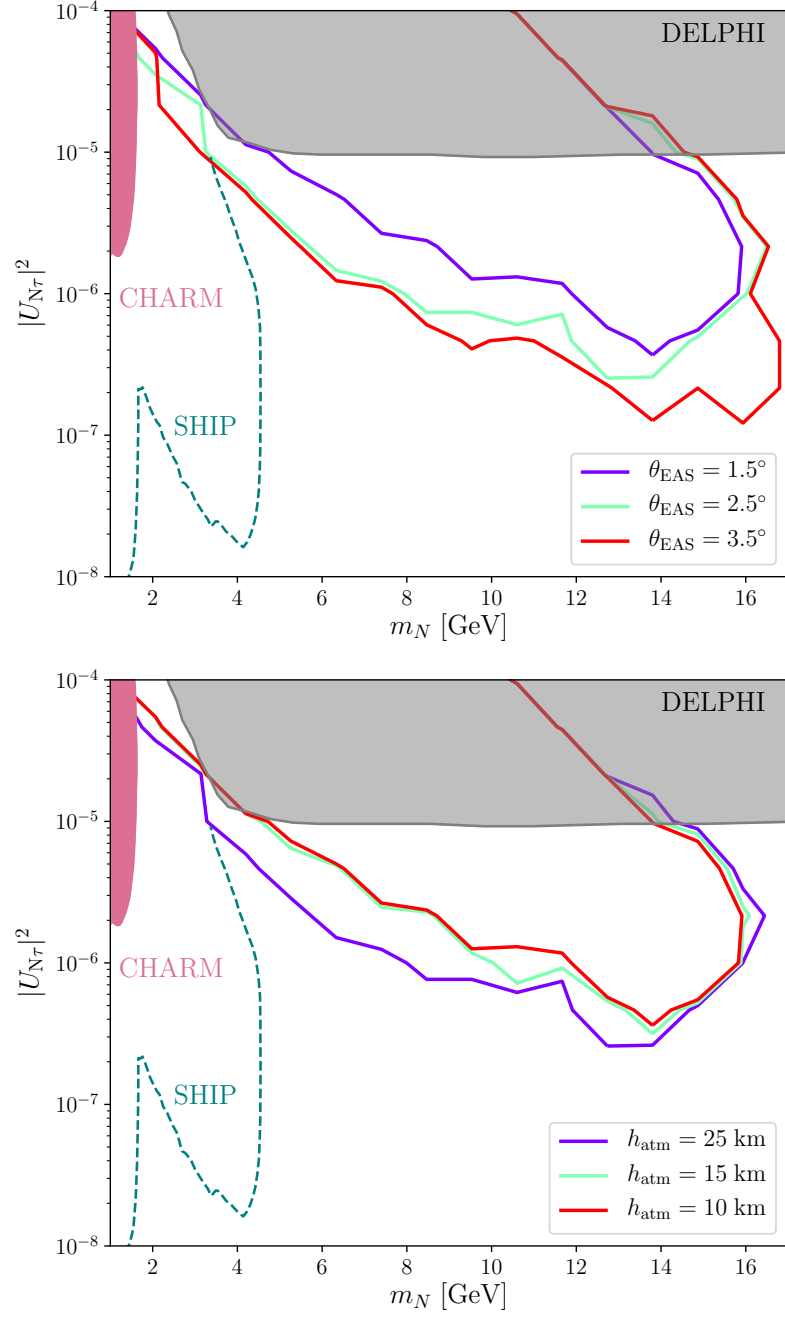


Figure 6.3: The sensitivity, as depicted in Fig. 6.2, for the case of $D = 50$ kpc with exit energies restricted to $10 \text{ EeV} \leq E_{\text{exit}} \leq 100 \text{ EeV}$, for differing values of the effective opening angle θ_{EAS} (first panel) and the atmospheric altitude h_{atm} (second panel)

Nonetheless, the regions probed are comparable enough that we consider the approximations used effective.

Chapter 7

Conclusions

7.1 Summary

In this thesis, we have explored the influence of BSM physics on the behaviour of UHE neutrinos as they traverse chords of the Earth, and the potential signals of such influence at large-volume observatories.

In particular, we considered the introduction of a right-handed Majorana neutrino of GeV-scale mass, mixing with the left-handed τ neutrino, and simulated the propagation of UHE neutrinos through the Earth in the presence of this BSM scenario with an adapted version of the `TauRunner` program, computing the exit probabilities of detectable daughter particles over a range of geometries. We then considered the production of observable extensive air showers by such particles, and modelled two detectors—namely GRAND, a ground-based radio array, and POEMMA, a satellite-based observatory—to estimate the effects on the numbers and energy distributions measured.

We found that, at small emergence angles corresponding to shallowly Earth-skimming particle tracks, the τ flux expected in the context of the Standard Model is considerably dominant over any BSM deviations. This severely limits the efficacy of GRAND, whose field of view is limited to small emergence angles by its geometry, for this

application. At deep emergence angles corresponding to long chords, however, the Earth becomes effectively opaque to UHE neutrinos in the Standard Model case, and the influence of the BSM physics can cause significant deviations in the detectable flux. These large emergence angles can be probed by POEMMA.

We contrasted a diffuse flux and astrophysical transients as sources of UHE neutrinos, and concluded that the diffuse flux was insufficient for this application. Assuming a flux comparable to that produced by GRB 221009A, we considered a similar transient event occurring at various distances from the Earth, and searched for regions of the model parameter space—scanning over RHN masses m_N and mixing angles θ_{mix} —where there would be deviations from the SM at a confidence level of 99.7%. This would probe unconstrained regions of the parameter space, with restrictions to various ranges of exit energy illuminating different subregions.

7.2 Further Study

To the knowledge of the author and his collaborators, this study was the first to propose testing for BSM scenarios involving long-lived intermediate particles, produced by an incoming (SM) UHE neutrino flux and propagating distances through the Earth, with large-volume detectors. This direction of study may hold a rich untapped potential for future analysis.

The RHN considered here mixes exclusively with the active τ neutrino, disregarding the lighter generations. A natural extension of this BSM model would be the inclusion of three flavours of right-handed neutrino, corresponding to the three flavours of left-handed neutrino and coupled to them via a larger mixing matrix in place of the single parameter θ_{mix} . A possibility for further study would be simulating the propagation of all flavours of lepton through the Earth in such a scenario.

In such a case, and indeed in consideration of the model explored here, it could be of interest to investigate the muon as a detectable particle alongside the τ , as the

distributions of Earth-exiting particles in their case have been shown to differ from the τ [83]. Another possibility is the tracking of the lighter neutrinos, ν_e and ν_μ , within the simulation, as they may provide secondary contributions to τ -induced EASes that were not accounted for here [102].

In principle, any theoretical setting in which Earth-traversing UHE neutrinos can produce relatively long-lived particles that propagate significant distances through the planet's interior could be apt for this avenue of study. A similar but more extensive BSM sector could include additional RHNs or, perhaps, the majoron: a Goldstone boson that, upon the spontaneous breaking of a global symmetry of lepton number, could provide the right-handed neutrino with a Majorana mass in the first place [103–105]. Scenarios wherein intermediate BSM particles are abundantly produced by an incoming UHE neutrino flux, but have shorter decay lengths than the RHN we considered, could be more significant for the results of detectors at lower altitudes than that of POEMMA, such as GRAND, PUEO, TAROGE-M, or Trinity. It could also be illuminating to apply our methods—in the context of both the model considered and perhaps the others suggested—to various other observatories, including both those listed and others on the horizon and in the future.

Another potential line of investigation could be the application of such simulations to other bodies in the Solar System in lieu of the Earth, allowing for variation in the sizes and density profiles available, though enacting the described detection techniques further afield would, of course, be subject to future space missions.

7.3 Closing Remarks

In conclusion, I have demonstrated in this thesis that, in the context of BSM theories wherein a long-lived intermediate particle produced by neutrino-nucleon interactions at ultra-high energy can propagate significant distances through the Earth, study of Earth-traversing UHE neutrinos at large-volume observatories could probe new physics. The simulations and methods applied here explore the case of a Majorana

right-handed neutrino of GeV-scale mass, and we conclude that the observations of high-altitude detectors like POEMMA should help to constrain the parameter space of such a theory.

This general framework could provide an interesting and illuminating avenue of study for the probing of physics beyond the Standard Model.

Bibliography

- [1] R. Heighton, L. Heurtier and M. Spannowsky, *Hunting for neutral leptons with ultra-high-energy neutrinos*, *Phys. Rev. D* **108** (Sep, 2023) 055009.
- [2] M. Ahlers, *High-energy cosmogenic neutrinos*, *Physics Procedia* **61** (2015) 392–398.
- [3] PARTICLE DATA GROUP collaboration, J. Beringer, J. F. Arguin, R. M. Barnett, K. Copic, O. Dahl, D. E. Groom et al., *Review of particle physics*, *Phys. Rev. D* **86** (Jul, 2012) 010001.
- [4] A. Rudolph, M. Petropoulou, W. Winter and Željka Bošnjak, *Multi-messenger Model for the Prompt Emission from GRB 221009A*, *The Astrophysical Journal Letters* **944** (Feb, 2023) L34.
- [5] F. Bergsma, J. Dorenbosch, M. Jonker, C. Nieuwenhuis, J. Allaby, U. Amaldi et al., *A search for decays of heavy neutrinos*, *Physics Letters B* **128** (1983) 361–366.
- [6] J. Orloff, A. Rozanov and C. Santoni, *Limits on the mixing of tau neutrino to heavy neutrinos*, *Physics Letters B* **550** (2002) 8–15.
- [7] DELPHI collaboration, P. Abreu et al., *Search for neutral heavy leptons produced in Z decays*, *Z. Phys. C* **74** (1997) 57–71.
- [8] SHiP collaboration, “Sensitivity of the SHiP experiment to Heavy Neutral Leptons.” <https://arxiv.org/abs/1811.00930>, 2019.

- [9] C. D. Anderson, *The Positive Electron*, *Phys. Rev.* **43** (Mar, 1933) 491–494.
- [10] J. C. Street and E. C. Stevenson, *New Evidence for the Existence of a Particle of Mass Intermediate Between the Proton and Electron*, *Phys. Rev.* **52** (Nov, 1937) 1003–1004.
- [11] C. M. G. Lattes, H. Muirhead, G. P. S. Occhialini and C. F. Powell, *Processes involving charged mesons*, *Nature* **159** (1947) 694–697.
- [12] R. Brown, U. Camerini, P. Fowler et al., *Observations with Electron-Sensitive Plates Exposed to Cosmic Radiation*, *Nature* **163** (1949) 82–87.
- [13] G. Aad, T. Abajyan, B. Abbott, J. Abdallah, S. Abdel Khalek, A. Abdelalim et al., *Observation of a new particle in the search for the Standard Model Higgs boson with the ATLAS detector at the LHC*, *Physics Letters B* **716** (Sept., 2012) 129.
- [14] PIERRE AUGER collaboration, *The Pierre Auger Cosmic Ray Observatory, Nuclear Instruments and Methods in Physics Research Section A: Accelerators, Spectrometers, Detectors and Associated Equipment* **798** (2015) 172–213.
- [15] M. Takita, *The Super-Kamiokande*, in *International Symposium on Neutrino Astrophysics*, pp. 135–145, 1992.
- [16] F. Halzen and S. R. Klein, *Invited Review Article: IceCube: An instrument for neutrino astronomy*, *Review of Scientific Instruments* **81** (08, 2010) 081101.
- [17] SUPER-KAMIOKANDE collaboration, Y. Fukuda, T. Hayakawa, E. Ichihara, K. Inoue, K. Ishihara, H. Ishino et al., *Evidence for Oscillation of Atmospheric Neutrinos*, *Phys. Rev. Lett.* **81** (Aug, 1998) 1562–1567.
- [18] SNO collaboration, Q. R. Ahmad, R. C. Allen, T. C. Andersen, J. D. Anglin, J. C. Barton, E. W. Beier et al., *Direct Evidence for Neutrino Flavor*

- Transformation from Neutral-Current Interactions in the Sudbury Neutrino Observatory, Phys. Rev. Lett.* **89** (Jun, 2002) 011301.
- [19] C. Deaconu, “Searches for Ultra-High Energy Neutrinos with ANITA.” <https://arxiv.org/abs/1908.00923>, 2019.
- [20] M. Ageron, J. Aguilar, I. Al Samarai, A. Albert, F. Ameli, M. André et al., *ANTARES: The first undersea neutrino telescope, Nuclear Instruments and Methods in Physics Research Section A: Accelerators, Spectrometers, Detectors and Associated Equipment* **656** (2011) 11–38.
- [21] J. Álvarez Muñiz, R. Alves Batista, A. Balagopal V., J. Bolmont, M. Bustamante, W. Carvalho et al., *The Giant Radio Array for Neutrino Detection (GRAND): Science and design, Science China Physics, Mechanics and Astronomy* **63** (Aug., 2019) .
- [22] A. Olinto, J. Krizmanic, J. Adams, R. Aloisio, L. Anchordoqui, A. Anzalone et al., *The POEMMA (Probe of Extreme Multi-Messenger Astrophysics) observatory, Journal of Cosmology and Astroparticle Physics* **2021** (June, 2021) 007.
- [23] A. G. Vieregge, Q. Abarr, P. Allison, J. Ammerman Yebra, J. Alvarez-Muñiz, J. J. Beatty et al., *Discovering the Highest Energy Neutrinos with the Payload for Ultrahigh Energy Observations (PUEO), PoS ICRC2021* (2021) 1029.
- [24] W. G. Thompson, “TAMBO: Searching for Tau Neutrinos in the Peruvian Andes.” <https://arxiv.org/abs/2308.09753>, 2023.
- [25] S.-H. Wang, J. Nam, P. Chen, Y. Chen, T. Choi, Y.-b. Ham et al., *TAROGEM: Radio Antenna Array on Antarctic High Mountain for Detecting Near-Horizontal Ultra-High Energy Air Showers, Journal of Cosmology and Astroparticle Physics* **2022** (Nov., 2022) 022.

- [26] A. M. Brown, M. Bagheri, M. Doro, E. Gazda, D. Kieda, C. Lin et al., “Trinity: An Imaging Air Cherenkov Telescope to Search for Ultra-High-Energy Neutrinos.” <https://arxiv.org/abs/2109.03125>, 2021.
- [27] ANITA collaboration, P. W. Gorham, J. Nam, A. Romero-Wolf, S. Hoover, P. Allison, O. Banerjee et al., *Characteristics of Four Upward-Pointing Cosmic-Ray-like Events Observed with ANITA*, *Phys. Rev. Lett.* **117** (Aug, 2016) 071101.
- [28] P. W. Gorham, B. Rotter, P. Allison, O. Banerjee, L. Batten, J. J. Beatty et al., *Observation of an Unusual Upward-Going Cosmic-Ray-like Event in the Third Flight of ANITA*, *Phys. Rev. Lett.* **121** (Oct, 2018) 161102.
- [29] A. Romero-Wolf, S. A. Wissel, H. Schoorlemmer, W. R. Carvalho, J. Alvarez-Muñiz, E. Zas et al., *Comprehensive analysis of anomalous ANITA events disfavors a diffuse tau-neutrino flux origin*, *Phys. Rev. D* **99** (Mar, 2019) 063011.
- [30] M. G. Aartsen, M. Ackermann, J. Adams, J. A. Aguilar, M. Ahlers, M. Ahrens et al., *A Search for IceCube Events in the Direction of ANITA Neutrino Candidates*, *The Astrophysical Journal* **892** (mar, 2020) 53.
- [31] L. Heurtier, Y. Mambrini and M. Pierre, *Dark matter interpretation of the ANITA anomalous events*, *Phys. Rev. D* **99** (May, 2019) 095014.
- [32] X. Liang and A. Zhitnitsky, *ANITA anomalous events and axion quark nuggets*, *Phys. Rev. D* **106** (Sep, 2022) 063022.
- [33] D. B. Fox, S. Sigurdsson, S. Shandera, P. Mészáros, K. Murase, M. Mostafá et al., “The ANITA Anomalous Events as Signatures of a Beyond Standard Model Particle, and Supporting Observations from IceCube.” <https://arxiv.org/abs/1809.09615>, 2018.

- [34] J. F. Cherry and I. M. Shoemaker, *Sterile neutrino origin for the upward directed cosmic ray showers detected by ANITA*, *Phys. Rev. D* **99** (Mar, 2019) 063016.
- [35] A. R. Zhitnitsky, ‘*Nonbaryonic*’ dark matter as baryonic colour superconductor, *Journal of Cosmology and Astroparticle Physics* **2003** (Oct, 2003) 010.
- [36] G.-Y. Huang, S. Jana, M. Lindner and W. Rodejohann, *Probing new physics at future tau neutrino telescopes*, *Journal of Cosmology and Astroparticle Physics* **2022** (Feb., 2022) 038.
- [37] S. L. Glashow, *Partial-symmetries of weak interactions*, *Nuclear Physics* **22** (1961) 579–588.
- [38] S. Weinberg, *A Model of Leptons*, *Phys. Rev. Lett.* **19** (Nov, 1967) 1264–1266.
- [39] A. Salam and J. C. Ward, *Weak and electromagnetic interactions*, *Il Nuovo Cimento* (1959) .
- [40] S. Weinberg, *The making of the Standard Model*, *The European Physical Journal C* **34** (May, 2004) 513.
- [41] D. Tong, “Lectures on the Standard Model.”
<https://www.damtp.cam.ac.uk/user/tong/standardmodel.html>, 2024.
- [42] P. W. Higgs, *Broken Symmetries and the Masses of Gauge Bosons*, *Phys. Rev. Lett.* **13** (Oct, 1964) 508–509.
- [43] PARTICLE DATA GROUP collaboration, S. Navas et al., *Review of particle physics*, *Phys. Rev. D* **110** (2024) 030001.
- [44] I. Sample, *The long story of how the boson got only Higgs’s name*, *Nature* **466** (2010) 689.

- [45] R. W. Gurney, *The number of particles in beta-ray spectra.II. Thorium B and thorium (C + D)*, *Proc. R. Soc. Lond. A* **112** (1926) 380–390.
- [46] J. Bromberg, *The Impact of the Neutron: Bohr and Heisenberg*, *Hist. Stud. Phys. Sci* **3** (1971) 307–341.
- [47] W. Pauli, *Letter: Dear Radioactive Ladies and Gentlemen*, 1930.
- [48] F. Reines and C. L. Cowan, *The neutrino*, *Nature* **178** (1956) 446–449.
- [49] D. Griffiths, *Historical Introduction to the Elementary Particles (Chapter 1: Introduction to Elementary Particles)*, pp. 13–58. Wiley-VCH, 2008.
- [50] F. W. Stecker, “Neutrino Physics and Astrophysics Overview.”
<https://arxiv.org/abs/2301.02935>, 2023.
- [51] R. Davis, *A Review of the Homestake Solar Neutrino experiment*, *Progress in Particle and Nuclear Physics* **32** (1994) 13–32.
- [52] M. Nakahata, “History of Solar Neutrino Observations.”
<https://arxiv.org/abs/2202.12421>, 2022.
- [53] T. Kajita, *Atmospheric neutrinos and discovery of neutrino oscillations*, *Proceedings of the Japan Academy, Series B* **86** (2010) 303–321.
- [54] Z. Maki, M. Nakagawa and S. Sakata, *Remarks on the Unified Model of Elementary Particles*, *Progress of Theoretical Physics* **28** (11, 1962) 870–880.
- [55] I. Esteban, M. C. Gonzalez-Garcia, M. Maltoni, I. Martinez-Soler, J. P. Pinheiro and T. Schwetz, *NuFit-6.0: updated global analysis of three-flavor neutrino oscillations*, *Journal of High Energy Physics* **2024** (Dec., 2024) .
- [56] M. Aker, A. Beglarian, J. Behrens, A. Berlev, U. Besserer, B. Bieringer et al., “First direct neutrino-mass measurement with sub-ev sensitivity.”
<https://arxiv.org/abs/2105.08533>, 2021.

- [57] S. F. King, *Neutrino mass models*, *Reports on Progress in Physics* **67** (Dec., 2003) 107157.
- [58] V. Brdar, A. J. Helmboldt, S. Iwamoto and K. Schmitz, *Type i seesaw mechanism as the common origin of neutrino mass, baryon asymmetry, and the electroweak scale*, *Phys. Rev. D* **100** (Oct, 2019) 075029.
- [59] A. Atre, T. Han, S. Pascoli and B. Zhang, *The Search for Heavy Majorana Neutrinos*, *JHEP* **05** (2009) 030, [0901.3589].
- [60] K. Greisen, *End to the Cosmic-Ray Spectrum?*, *Phys. Rev. Lett.* **16** (Apr, 1966) 748–750.
- [61] G. T. Zatsepin and V. A. Kuzmin, *Upper limit of the spectrum of cosmic rays*, *JETP Lett.* **4** (1966) 78–80.
- [62] HIGH RESOLUTION FLY’S EYE collaboration, R. U. Abbasi, T. Abu-Zayyad, M. Allen, J. F. Amman, G. Archbold, K. Belov et al., *First observation of the greisen-zatsepin-kuzmin suppression*, *Phys. Rev. Lett.* **100** (Mar, 2008) 101101.
- [63] PIERRE AUGER collaboration, J. Abraham, P. Abreu, M. Aglietta, C. Aguirre, D. Allard, I. Allekotte et al., *Observation of the suppression of the flux of cosmic rays above 4×10^{19} eV*, *Phys. Rev. Lett.* **101** (Aug, 2008) 061101.
- [64] H. Athar, M. Jezabek and O. Yasuda, *Effects of neutrino mixing on high-energy cosmic neutrino flux*, *Phys. Rev. D* **62** (Oct, 2000) 103007.
- [65] ANITA collaboration, P. W. Gorham, P. Allison, O. Banerjee, L. Batten, J. J. Beatty, K. Bechtol et al., *Constraints on the diffuse high-energy neutrino flux from the third flight of ANITA*, *Phys. Rev. D* **98** (Jul, 2018) 022001.
- [66] ICECUBE 2 collaboration, M. G. Aartsen, M. Ackermann, J. Adams, J. A. Aguilar, M. Ahlers, M. Ahrens et al., *Differential limit on the*

- extremely-high-energy cosmic neutrino flux in the presence of astrophysical background from nine years of IceCube data*, *Phys. Rev. D* **98** (Sep, 2018) 062003.
- [67] A. Aab, P. Abreu, M. Aglietta, I. Albuquerque, J. Albury, I. Allekotte et al., *Probing the origin of ultra-high-energy cosmic rays with neutrinos in the EeV energy range using the Pierre Auger Observatory*, *Journal of Cosmology and Astroparticle Physics* **2019** (oct, 2019) 022.
- [68] C. Guépin, K. Kotera and F. Oikonomou, “High-energy neutrino transients and the future of multi-messenger astronomy.”
<https://arxiv.org/abs/2207.12205>, 2022.
- [69] Y.-F. Yuan and X.-Y. Shi, *Collision of ultra-relativistic proton with strong magnetic field: Production of ultra-high energy photons and neutrinos*, *Physics Letters B* **795** (2019) 452–456.
- [70] LIGO SCIENTIFIC COLLABORATION AND VIRGO collaboration, B. P. Abbott, R. Abbott, T. D. Abbott, M. R. Abernathy, F. Acernese, K. Ackley et al., *Observation of Gravitational Waves from a Binary Black Hole Merger*, *Phys. Rev. Lett.* **116** (Feb, 2016) 061102.
- [71] ANTARES AND ICECUBE AND LIGO SCIENTIFIC COLLABORATION AND VIRGO collaboration, S. Adrián-Martínez, A. Albert, M. André, M. Anghinolfi, G. Anton, M. Ardid et al., *High-energy neutrino follow-up search of gravitational wave event GW150914 with ANTARES and IceCube*, *Phys. Rev. D* **93** (Jun, 2016) 122010.
- [72] R. Abbasi, M. Ackermann, J. Adams, J. A. Aguilar, M. Ahlers, M. Ahrens et al., *Follow-up of Astrophysical Transients in Real Time with the IceCube Neutrino Observatory*, *The Astrophysical Journal* **910** (mar, 2021) 4.
- [73] J. A. Formaggio and G. P. Zeller, *From eV to EeV: Neutrino cross sections across energy scales*, *Rev. Mod. Phys.* **84** (Sep, 2012) 1307–1341.

- [74] C. Giunti and C. W. Kim, *Fundamentals of Neutrino Physics and Astrophysics*, p. 167. Oxford University Press, 2007.
10.1093/acprof:oso/9780198508717.001.0001.
- [75] J.-H. Koehne, K. Frantzen, M. Schmitz, T. Fuchs, W. Rhode, D. Chirkin et al., *PROPOSAL: A tool for propagation of charged leptons*, *Computer Physics Communications* **184** (2013) 2070–2090.
- [76] J. Alvarez-Muñiz, W. R. Carvalho, K. Payet, A. Romero-Wolf, H. Schoorlemmer and E. Zas, *Comprehensive approach to tau-lepton production by high-energy tau neutrinos propagating through the Earth*, *Phys. Rev. D* **97** (Jan, 2018) 023021.
- [77] R. M. Abraham, J. Alvarez-Muñiz, C. A. Argüelles, A. Ariga, T. Ariga, A. Aurisano et al., *Tau neutrinos in the next decade: from GeV to EeV*, *Journal of Physics G: Nuclear and Particle Physics* **49** (oct, 2022) 110501.
- [78] I. Safa, J. Lazar, A. Pizzuto, O. Vasquez, C. A. Argüelles and J. Vandenbroucke, *TauRunner: A public Python program to propagate neutral and charged leptons*, *Computer Physics Communications* **278** (2022) 108422.
- [79] A. M. Dziewonski and D. L. Anderson, *Preliminary reference Earth model*, *Physics of the Earth and Planetary Interiors* **25** (1981) 297–356.
- [80] T. K. Gaisser, R. Engel and E. Resconi, *Extensive air showers*, pp. 313–340. Cambridge University Press, 2016.
- [81] T. M. Venters, M. H. Reno, J. F. Krizmanic, L. A. Anchordoqui, C. Guépin and A. V. Olinto, *POEMMAs target-of-opportunity sensitivity to cosmic neutrino transient sources*, *Physical Review D* **102** (Dec., 2020) .
- [82] M. H. Reno, J. F. Krizmanic and T. M. Venters, *Cosmic tau neutrino detection via Cherenkov signals from air showers from Earth-emerging taus*, *Phys. Rev. D* **100** (Sep, 2019) 063010.

- [83] A. L. Cummings, R. Aloisio and J. F. Krizmanic, *Modeling of the tau and muon neutrino-induced optical Cherenkov signals from upward-moving extensive air showers*, *Phys. Rev. D* **103** (Feb, 2021) 043017.
- [84] K. R. Dienes and B. Thomas, *Dynamical dark matter. I. Theoretical overview*, *Phys. Rev. D* **85** (Apr, 2012) 083523.
- [85] K. R. Dienes, L. Heurtier, F. Huang, D. Kim, T. M. P. Tait and B. Thomas, *Stasis in an expanding universe: A recipe for stable mixed-component cosmological eras*, *Phys. Rev. D* **105** (Jan, 2022) 023530.
- [86] A. Pilaftsis, *Leptogenesis in theories with large extra dimensions*, *Phys. Rev. D* **60** (Oct, 1999) 105023.
- [87] K. R. Dienes, E. Dudas and T. Gherghetta, *Light neutrinos without heavy mass scales: a higher-dimensional seesaw mechanism*, *Nuclear Physics B* **557** (1999) 25–59.
- [88] LIGO SCIENTIFIC COLLABORATION AND VIRGO collaboration, B. P. Abbott, R. Abbott, T. D. Abbott, F. Acernese, K. Ackley, C. Adams et al., *GW170817: Observation of Gravitational Waves from a Binary Neutron Star Inspiral*, *Phys. Rev. Lett.* **119** (Oct, 2017) 161101.
- [89] E. Waxman, *Cosmological Gamma-Ray Bursts and the Highest Energy Cosmic Rays*, *Phys. Rev. Lett.* **75** (Jul, 1995) 386–389.
- [90] M. Vietri, *The Acceleration of Ultra-High-Energy Cosmic Rays in Gamma-Ray Bursts*, **453** (Nov., 1995) 883, [[astro-ph/9506081](#)].
- [91] P. Veres, E. Burns, E. Bissaldi, S. Lesage, O. Roberts and Fermi GBM Team, *GRB 221009A: Fermi GBM detection of an extraordinarily bright GRB, GRB Coordinates Network* **32636** (Oct., 2022) 1.

- [92] S. Dichiara, J. D. Gropp, J. A. Kennea, N. P. M. Kuin, A. Y. Lien, F. E. Marshall et al., *Swift J1913.1+1946 a new bright hard X-ray and optical transient*, *The Astronomer's Telegram* **15650** (Oct., 2022) 1.
- [93] R. Pillera, E. Bissaldi, N. Omodei, G. La Mura, F. Longo, F.-L. team et al., *GRB 221009A: Fermi-LAT refined analysis*, *GRB Coordinates Network* **32658** (2022) 1.
- [94] Y. Huang, S. Hu, S. Chen, M. Zha, C. Liu, Z. Yao et al., *LHAASO observed GRB 221009A with more than 5000 VHE photons up to around 18 TeV*, *GRB Coordinates Network* **32677** (Oct., 2022) 1.
- [95] A. de Ugarte Postigo, L. Izzo, G. Pugliese, D. Xu, B. Schneider, J. P. U. Fynbo et al., *GRB 221009A: Redshift from X-shooter/VLT*, *GRB Coordinates Network* **32648** (Oct., 2022) 1.
- [96] R. A. Batista, “GRB 221009A: a potential source of ultra-high-energy cosmic rays.” <https://arxiv.org/abs/2210.12855>, 2022.
- [97] ICECUBE collaboration, *GRB 221009A: Upper limits from a neutrino search with IceCube*, *GRB Coordinates Network* **32665** (Oct., 2022) 1.
- [98] M. Ackermann, S. K. Agarwalla, J. Alvarez-Muñiz, R. A. Batista, C. A. Argüelles, M. Bustamante et al., “High-Energy and Ultra-High-Energy Neutrinos.” <https://arxiv.org/abs/2203.08096>, 2022.
- [99] K. Cheung, Y.-L. Chung, H. Ishida and C.-T. Lu, *Sensitivity reach on heavy neutral leptons and τ -neutrino mixing $|U_{\tau N}|^2$ at the HL-LHC*, *Phys. Rev. D* **102** (Oct, 2020) 075038.
- [100] O. Fischer, B. Pattnaik and J. Zurita, *Testing Heavy Neutral Leptons in Cosmic Ray Beam Dump experiments*, *Journal of High Energy Physics* **2023** (July, 2023) .

-
- [101] L. Heurtier and Y. Zhang, *Supernova constraints on massive (pseudo)scalar coupling to neutrinos*, *Journal of Cosmology and Astroparticle Physics* **2017** (Feb., 2017) 042042.
- [102] A. G. Soto, P. Zhelnin, I. Safa and C. A. Argüelles, *Tau Appearance from High-Energy Neutrino Interactions*, *Phys. Rev. Lett.* **128** (Apr, 2022) 171101.
- [103] Y. Chikashige, R. Mohapatra and R. Peccei, *Are there real goldstone bosons associated with broken lepton number?*, *Physics Letters B* **98** (1981) 265–268.
- [104] J. Schechter and J. W. F. Valle, *Neutrino decay and spontaneous violation of lepton number*, *Phys. Rev. D* **25** (Feb, 1982) 774–783.
- [105] J. Heeck, “Phenomenology of Majorons.”
<https://arxiv.org/abs/1709.07670>, 2017.